ARTICLE

https://doi.org/10.1590/2317-4889202220210041

BJGEO Brazilian Journal of Geology

Post-Cretaceous brittle tectonics in the Tunas Alkaline Complex, Paraná, Brazil

Taily Ferreira Santos Farias[1]*, Eduardo Salamuni[1], William Rudolf Lopes Peyerl[1], Viviane Barbosa Gimenez[1]

Abstract

We present a study of the brittle tectonics of Tunas Alkaline Complex focusing on the kinematic and geometric analysis of faults and brittle shear zones deforming the complex. The data acquired and respective interpretations sought to contribute to the post-Cretaceous tectonic structural models of southern Brazil. The ~83 Ma-old alkaline complex is made up of syenites, alkali syenites, plutonic and volcanic breccias, as well as trachyte, microsyenite, and bostonite dykes. Morphostructural analysis using remote sensing combined with right dihedral kinematic analysis of fault-slip data and relations of intersections among structures allowed us to characterize four Cenozoic paleostress fields and their respective tectonic pulses: (I) Eocene-Oligocene NW-SE extension responsible for normal oblique-slip faults striking N60-70E; (II) Oligocene-Miocene NE-SW compression associated with tectonic accommodation of the South American Plate at circa 27–26 Ma, and responsible for WNW-ESE-trending sinistral and NE-SW-trending dextral strike-slip faults; (III) Plio-Pleistocene N-S to NNW-SSE compression related to dextral reactivation of NW-SE-striking faults, sinistral reactivation of NE-SW-trending faults, and generation of NNW-SSE-trending strike-slip faults; and (IV) Pleistocene-Holocene NW-SE to WNW-ESE compression that caused dextral reactivation of ENE-WSW-trending faults and sinistral strike-slip reactivation of NNW-SSE-trending faults.

KEYWORDS: Alkaline rocks; brittle tectonics; Cenozoic deformation; strike-slip faults; paleostress.

INTRODUCTION

In this research, a structural analysis was performed to find the stress fields responsible for the deformation recorded in the Tunas Alkaline Complex (TAC), an alkaline massif located in the southeastern Brazil, in order to determine the tectonic pulses related to that deformation. It was possible to establish the structural framework and the orientations of paleostress fields (tectonic pulses I, II, III, and IV) related to the reactivation of faults along the main axis of the Ponta Grossa Arch, which comprises a structure linked to the evolution of the Brazilian Continental Shelf. The results provided a structural interpretation of the TAC faults, a massif that is part of the chronologically (~83 Ma) correlated set of alkaline rocks controlled by the referred arch (Ferreira *et al.* 1981, Siga Jr. *et al.* 2007). The research was based on the geometric and kinematic structural analysis of faults observed in outcrops in addition to photointerpretation of aerial photographs and satellite imagery, which allowed us to obtain interpretations regarding the sequence of tectonic pulses that affected the TAC. Due to their ages and the homogeneity of their lithotypes, the alkaline rocks are important sites for the study and understanding of the Cenozoic tectonic evolution of the Brazilian Shelf.

In this regard, the Juro-Cretaceous Wealdenian tecto-no-magmatic reactivation (Almeida 1967, Brito-Neves 1992) was responsible for extensional tectonic processes during the separation of the South American and African Tectonic Plates (Coutinho 2008, Will and Frimmel 2018). The resulting stress, which affected the South American Plate during and after the breakup of Gondwana and the opening of the South Atlantic Ocean, directly or indirectly controlled not only the emplacement of basic rocks such as those creating swarms of dykes across the Ponta Grossa Arch but also intrusion of the TAC and other alkaline complexes with posterior deformation associated.

The largest alkaline complex in southern Brazil is the TAC, emplaced into Precambrian rocks of the Ribeira Belt along the Ponta Grossa Arch in eastern Paraná (Gomes *et al.* 2011, 2018). Alkaline complexes of southern and southeastern Brazil comprise fine-grained syenitic and mafic-ultramafic rocks occurring as plugs, dykes, and veins (Gomes *et al.* 2011). As initial markers of local tectonic pulses, the Cretaceous microsyenite dykes of the complex vary in age between 81.1 ± 1.1 Ma (K/Ar, Gomes *et al.* 1987) and 84.7 ± 1.2 Ma (U/Pb–SHRIMP, Siga Jr. *et al.* 2007).

Supplementary data

Supplementary data associated with this article can be found in the online version: Supplementary Material 1; Supplementary Material 2; Supplementary Material 3.

[1]Universidade Federal do Paraná – Curitiba (PR), Brasil. E-mails: tailygeo@gmail.com, salamuni@ufpr.br, will.lopes.peyerl@gmail.com, vivianebgimenez@yahoo.com.br

*Corresponding author.

From a structural and geodynamic standpoint, these alkaline complexes are valuable indicators of Upper and post-Cretaceous tectonics; they frequently record the entire chain of events, from intrusion to final deformation stages, establishing the morphostructural framework of southern and southeastern Brazil. In such areas, drainage systems and topography reveal uplift, river capture, and block rotation, which are usual indicators of recent tectonic activity (Cobbold *et al*. 2001, Peyerl *et al*. 2018, Santos *et al*. 2019). The Neogene and younger deformation features are neotectonic in character, given the deformation they imprint on current topography (Hasui 1990, Peyerl *et al*. 2018).

Low-magnitude seismic events have been recorded in the surroundings of the TAC, presumably related to the relatively slow tectonic evolution of the region. A M3.1 (body wave magnitude) seism was observed in Tunas do Paraná city in 2015 and in 2016, and M2.8 was recorded in Bocaiúva do Sul city. Two events of M2.5 and M2.8 took place in Rio Branco do Sul city in 2013 (Sismo-IAG-USP 2018). In 2017, three seismic events of M3.5 were recorded near Tunas do Paraná, one of which was located between Rio Branco do Sul and Itaperuçu cities (University of Brasilia Seismologic Observatory — ObSis 2018, Sismo-IAG-USP 2018).

According to Lima (2000), this intraplate seismicity reflects neotectonic events, being partially attributed to recent reactivation of Proterozoic suture zones. Intraplate seismic distribution models consider the weak zones and accumulation of stress from lateral density variation or flexure preferentially across areas where Upper Cretaceous alkaline rocks outcrop (Assumpção *et al*. 2014). As only minor intraplate tectonic change has been observed in the region since the Lower Paleogene, the aforementioned seismic events indicate Cenozoic reactivation of ancient faults.

The local structural setting along the northern border of the São Jerônimo-Curiúva Lineament (Zalán *et al*. 1987) in the Ponta Grossa Arch is of fundamental importance for the comprehension of the Cretaceous and post-Cretaceous tectonics affecting the complex. Regional studies (Ferreira *et al*. 1981, Amaral 1982, Ferreira 1982, Trzaskos 2006, Franco-Magalhães *et al*. 2010a, 2010b, Strugale *et al*. 2007, Karl *et al*. 2013, Castro and Ferreira 2015, Morales *et al*. 2017) provide a sound understanding of the tectonic and structural framework of the Maringá-Curitiba Fault Zone and, therefore, the country rocks.

Given the Campanian age of the TAC, between 82.2 and 82.7 Ma (Gomes *et al*. 1987, Siga Jr. *et al*. 2007), the structural lineaments resulting from brittle deformation of alkaline plugs can overall be considered to have been nucleated during the Cenozoic or at least in the Late Cretaceous.

An investigation into the geometry and kinematics of post-Cretaceous faulting on TAC was performed to clarify its deformation history and its possible relations with older, country rock faults. In this way, we present a geometric analysis of brittle structures such as joints, faults, striation features, and well-exposed kinematic indicators, as well as their kinematic and dynamic interpretations, mainly at quarries.

The research aimed to identify the faults that cut the TAC and establish a relative chronology from their geometry and kinematics. Paleostress fields responsible for the deformation of the complex and their relations with previously studied regional stress fields in southern and southeastern Brazil were determined (Mancini and Riccomini 1994, Riccomini 1995, Salvador and Riccomini 1995, Riccomini and Assumpção 1999, Salamuni *et al*. 1999, 2004, Lima 2000, Hiruma *et al*. 2001, Chiessi and Riccomini 2003, Riccomini *et al*. 2004, Trzaskos 2006, Strugale *et al*. 2007, Chavez-Kus and Salamuni 2008, Hiruma *et al*. 2010, Jacques *et al*. 2010, Silva and Mello 2011, Machado *et al*. 2012, Nummer *et al*. 2014, Moura and Riccomini 2017, Peyerl *et al*. 2018). In addition, low-temperature thermochronological data, especially from Apatite Fission Track (AFT; Gallagher *et al*. 1994, Hadler *et al*. 2001, Hackspacher *et al*. 2004, Franco-Magalhães *et al*. 2010a, 2010b, Hiruma *et al*. 2010, Cogné *et al*. 2011, Siqueira-Ribeiro *et al*. 2012, Engelmann de Oliveira *et al*. 2018) were used as relative geochronological markers among the tectonic pulses interpreted from structural data.

Our goal is to contribute to the Cenozoic tectono-structural modeling of southern and southeastern Brazil by investigating local intraplate tectonics and extend our interpretations to a regional context of events.

Several studies were carried out in the context of Cenozoic tectonics of southeastern Brazil; however, those restricted to the alkaline rocks of the Ponta Grossa Arch are scarce. In this context, this article presents a contribution to the intraplate tectonic interpretations related to the Curitiba-Maringá Fault Zone, especially regarding to the understanding of the local paleostresses. Moreover, our proposal of a local tectono-structural model may also be applicable in studies aimed at mineral prospecting, groundwater research, and hydrocarbon exploration within the offshore arc domain.

STUDY AREA

The study area is located 80 km to the north of Curitiba city (Fig. 1) and extends over parts of Tunas do Paraná and Cerro Azul cities. The main access routes to the visited outcrops are the BR-476, known as Ribeira highway, crossing the region from north to south, and the PR-340, which borders the TAC from southeast to northwest. The massif is limited by latitudes 24°58'58" S and 24°54'56" S and longitude 49°03'05" W and 49°07'35" W.

MATERIALS AND METHODS

For the present study, we considered lineaments to correspond to either collective or isolated features that can be attributed to morphostructures, such as river segments along rectilinear crests or valleys. Lineaments are rectilinear or slightly curved elements generally associated with geological elements that correspond to structural weakness directions as defined by O'Leary *et al*. (1976). The hillshade map (Fig. 2) was constructed from work performed on ALOS Palsar Global Digital Elevation Model (ALOS-GDEM) and the geological map of the TAC depicting faults and lineaments was interpreted from ASTER-GDEM (Global Digital Elevation Model-Advanced

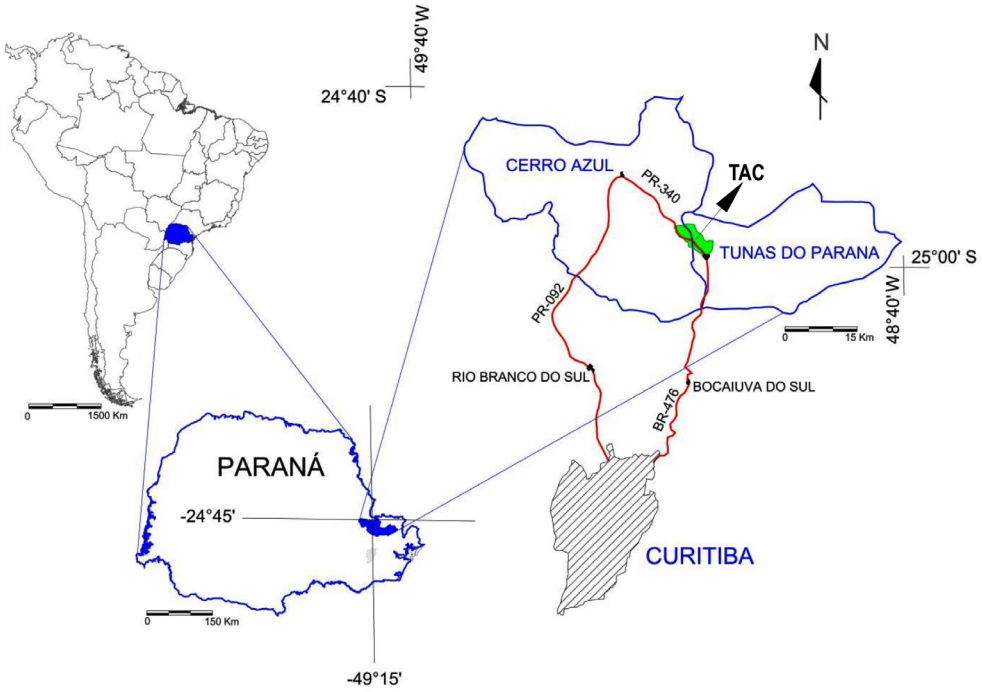

Figure 1. Localization map of the TAC: The complex is represented in red, being approximately 80 km to the north of Curitiba city in Paraná, Brazil. Access routes are the BR-476 and the PR-340 highways.

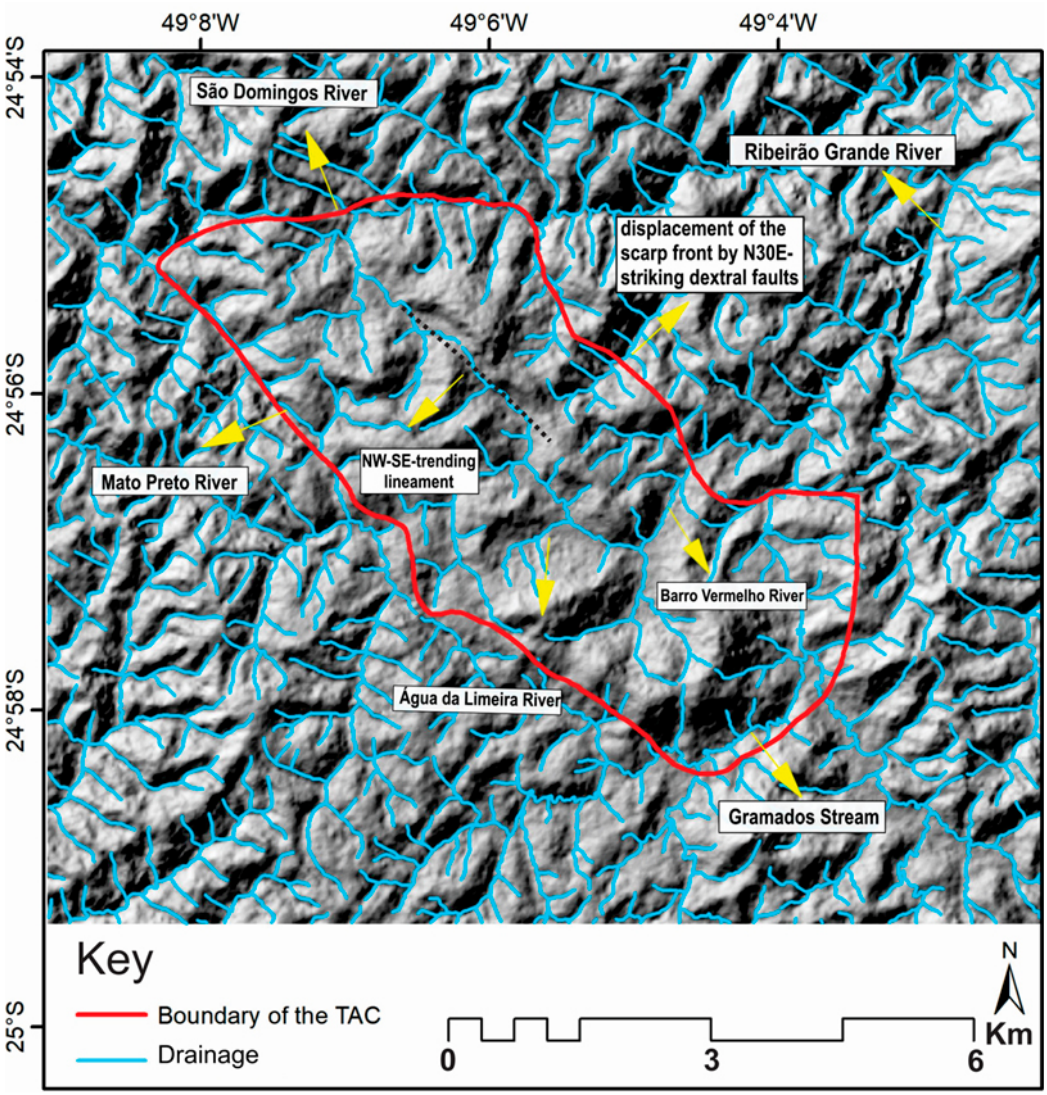

Figure 2. The local drainage map of TAC: TAC's drainage map (hillshade map) and its surroundings were superimposed on an ALOS Palsar Global Digital Elevation Model (ALOS-GDEM) of the area. The red line marks the boundary of the complex and the blue line marks the hydrographic segments (rivers and streams).

Spaceborne Thermal Emission and Reflection Radiometer) data in Global Mapper software (download of the images) and ArcGIS software v. 10.0 (interpretations of hillshade map). In the ArcGIS software, we extracted hillshade maps which were constructed by setting light sources at azimuths 45°, 180°, and 315° so that structures oriented to all quadrants could be emphasized. In this way, 1:100,000 and 1:50,000 lineament maps were obtained.

The 1:50,000 structural lineament map was traced from 1:70,000 aerial photos, and the drainage lineament map was derived from a 1:50,000 topographical map (by Water and Earth Institute *after* Institute of Land, Cartography and Geosciences of Paraná State). We interpreted the 1:400,000 and 1:50,000 magnetometric lineament maps using Analytical Signal Inclination – Total Horizontal Gradient (ASI-THG; Ferreira *et al*. 2010, Ferreira *et al*. 2013) analysis of preprocessed data by Geological Survey of Brazil (CPRM 2011). The frequency (azimuth) and length (coordinates X and Y) rose diagrams were obtained by using map calculation tools in ArcMap and RockWorks software. Thus, the structures were classified for posterior identification of their prominent structural trends in the complex.

We studied 23 outcrops, mainly at active or decommissioned quarries and highway cuttings, obtaining 358 joint and fault readings (Suppl. Mat. 1). The Riedel conjugate structures and fault block kinematic indicators (Tjia 1964, Petit 1987, Doblas 1998) were additionally investigated. To accomplish the structural analysis data were joined, in the Wintensor software (Delvaux 2012), at nine angular intervals so that the analysis was as compatible as possible with the "Riedel" fracturing model. Therefore, there are joint and failure systems according to the following intervals:

- N9E- to N9W-striking faults;
- N10W- to N29W-striking faults;
- N30W- to N49W-striking faults;
- N50W- to N69W-striking faults;
- N70W- to N90W-striking faults;
- N10E- to N29E-striking faults;
- N30E- to N49E-striking faults;
- N50E- to N69E-striking faults;
- N70E- to N90E-striking faults.

This families were used to interpret statistically the structures cataloged and based on that we define the most important structural trends in TAC area.

The fault families were classified as normal, dextral, or sinistral (Table 1) so that paleostress fields could be calculated using Wintensor software (Delvaux 2012) by applying the right dihedral method of Angelier and Mechler (1977). Those structures, as well as fault intersections and occasional striae overlapping relations, were described in detail.

The right dihedron graphic showing paleostress field directions was generated in the Wintensor software using the Auto Reject tool, which refines the database considering only fault directions showing slickensides/slickenlines and another kinematic indicators. Thus, out of a total of 358 fractures measurements, only 115 were considered for analysis. In Data Separation and Dieder Processing, those with the best statistical results were tested and their indicators were expressed in the R. Dihedron graphic resulting, only comprising faults that could be activated under a predetermined paleostress field.

Energy-dispersive X-ray spectroscopy (EDXS) was applied under scanning electron microscopy (SEM) to three samples

Table 1. In the Wintensor software (Delvaux 2012), the faults with reliable kinematic indicators were classified as follows: (1) the N30-60E-striking faults classified as 1.1 when normal, 1.2 when dextral, and 1.3 when sinistral; (2) the N30W-N30E-striking faults were classified as 2.1 when normal, 2.2 when dextral, and 2.3 when sinistral; (3) the N30W-N60W-striking faults were classified as 3.1 when normal, 3.2 when dextral, and 3.3 when sinistral; and (4) N60-90E- and N60-90W-striking faults were classified as 4.1 when normal, 4.2 when dextral, and 4.3 when sinistral. This classification was adopted as a premise for the Wintensor software that works with the measures of fault plans, slickensides, or slickenlines and kinematic indicators observed in the field. From a total of 358 fault and joint measurements, only the fault plane data with determinable kinematics were considered, resulting in a final database of 115 measurements.

Faults with reliable kinematic indicators			
WINTENSOR input data	**Normal faults**	**Dextral strike-slip faults**	**Sinistral strike-slip faults**
1-Faults	N30-60E-trending faults	N30-60E-trending faults	N30-60E-trending faults
Input data	1.1	1.2	1.3
N	9	10	15
2-Faults	N30W-N30E-trending faults	N30W-N30E-trending faults	N30W-N30E-trending faults
Input data	2.1	2.2	2.3
N	4	5	16
3-Faults	N30-60W-trending faults	N30-60W-trending faults	N30-60W-trending faults
Input data	3.1	3.2	3.3
N	3	4	4
4-Faults	E-W-trending faults	E-W-trending faults	E-W-trending faults
Input data	4.1	4.2	4.3
N	3	12	30

of fault planes showing clay mineral recrystallization at the Rock and Mineral Analysis Laboratory at the Universidade Federal do Paraná (LAMIR-UFPR) in order to identify the morphological framework in which mineral recrystallization affects specific fault planes. The minerals in recrystallized fault planes were identified by powder X-ray diffraction (XRD; Suppl. Mat. 2) following the laboratory specifications in Suppl. Mat. 2. The brittle structural and tectonic data obtained in this research were analyzed in the light of the literature on the post-Cretaceous brittle tectonics of southern and southeastern Brazil and were contrasted with published AFT data in order to establish the correlations among cooling and heating events and the tectonic deformation which acted in the TAC.

MORPHOSTRUCTURAL AND GEOLOGICAL SETTINGS

Morphostructures

In the TAC, morphostructures are mainly controlled by NW-SE- and NE-SW-striking faults, showing crests and valleys preferentially oriented to N45-60W and N40-50E striking (Figs. 2 and 3), with one of them partially marking the complex in its northeast boundary. The N10-20E- and N40-60E-trending drainage lineaments normally control short (about 250 m length) drainage segments, whereas segments aligned to N40-60W trend may extend for as long as 500 m.

The more extensive photointerpreted lineaments are oriented in NE-SW and NW-SE directions, followed by E-W ones. The NW-SE-trending lineaments, which are parallel to the São Jerônimo-Curiúva Lineament, were more prominently noticed, also controlling a river segment that cuts through the central portion of the complex at the foothill of a dissected scarp (Fig. 2). The capture and the displacement of the scarp front by N30E-striking dextral faults were also observed. Such characteristics may possibly correspond to morphotectonic processes that operated in a relatively recent structural context. The dissection of the complex was controlled by lineaments, with thin eroded soil beds and colluvial deposits of variable thicknesses. The drainage systems of the complex follow a trellis pattern, with some local dendritic remnants.

Geological and tectonic framework

The alkaline complexes of the Upper Cretaceous of the Ribeira valley region are tectonically related to the São Jerônimo-Curiúva Lineament (Siga Jr. *et al.* 2007) and Curitiba-Maringá Fault Zone (Figs. 4 and 5). They are generally oriented in the NW-SE direction and intersect NE-SW-striking structures affecting metasedimentary rocks of the Açungui Group. To the southeast of the study area, the Lancinha-Cubatão Shear Zone (Figs. 4 and 5) stands out as an important morphostructure oriented in the N45-50E direction, being part of the Além-Paraíba-Cubatão-Lancinha Lineament (Sadowski and Motidome 1987). According to Fassbinder *et al.* (1992), this

Figure 3. TAC's geomorphology: (A) E-W-trending crests and valleys; (B) SW-NE view of NW-SE-trending crests.

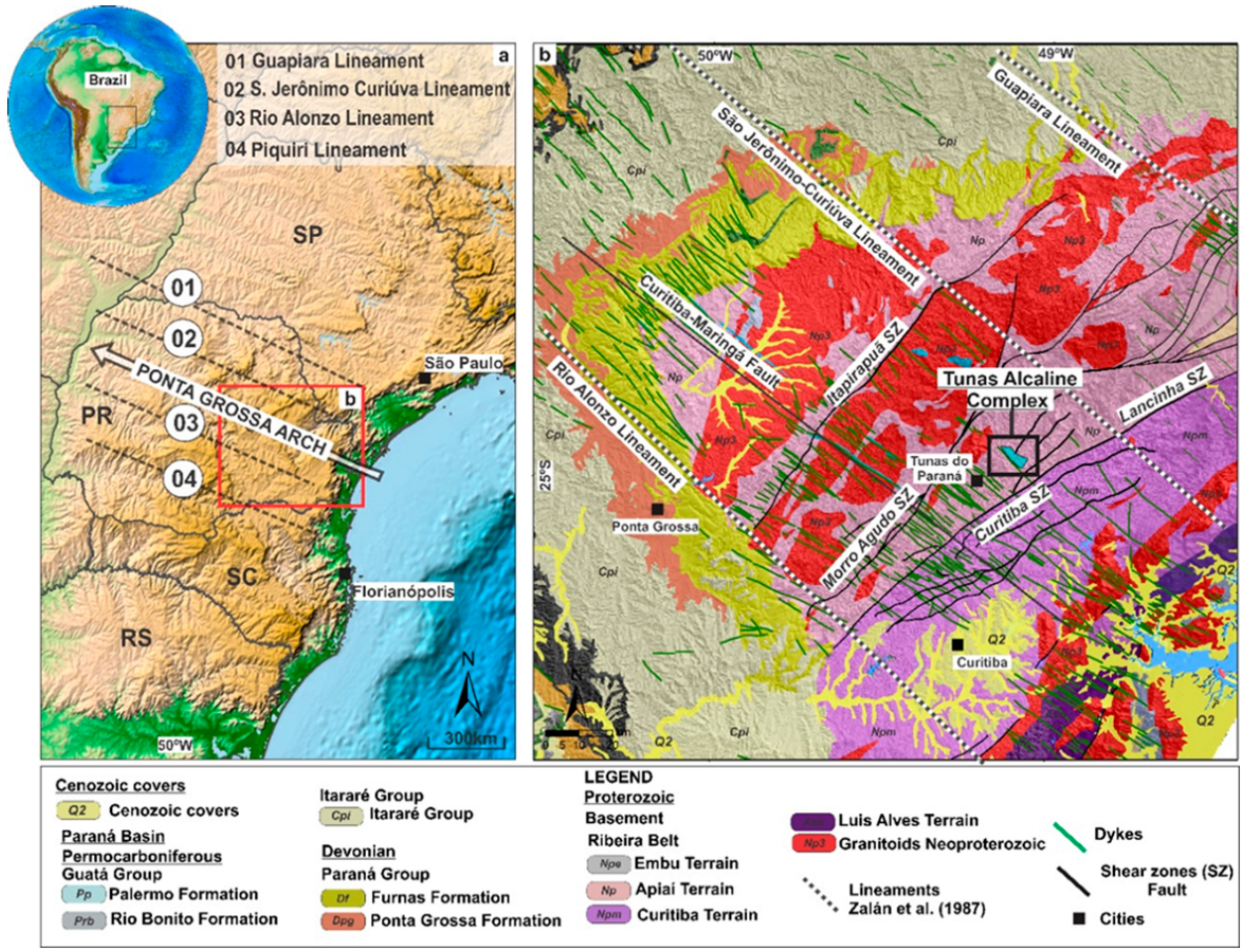

Source: based in Zalán *et al.* (1987).

Figure 4. TAC, PGA, and principal fault zones: simplified geological and structural map of the central region of Ponta Grossa Arch, with the location of the TAC, the São Jerônimo-Curiúva Lineament and the Curitiba-Maringá Fault Zone, among other lineaments and faults.

shear zone is identified by two deformation events, a ductile in the Neoproterozoic and a subsequent brittle/ductile one with widespread fracturing and associated breccias. The TAC was emplaced into Mesoproterozoic phyllites of the Votuverava Formation (Açungui Group), as well as into quartzites and schists of the Setuva Complex (Figs. 4 and 6).

Another important regional structural zone is the São Jerônimo-Curiúva Lineament (Figs. 4 and 5A), which displays Devonian to Juro-Cretaceous activity (Strugale *et al.* 2007). The extensional tectonics which this lineament was associated with was also responsible for fractures generally oriented to the N45W direction and filled by massive swarms of tholeiitic diabase dykes in the Cretaceous.

The TAC consists of a set of plugs whose lithotypes are hornblende syenite and hornblende quartz syenite, as well as phonolites, volcanic breccias, trachytes, alkaline gabbros, and, secondarily, diorites, monzodiorites, and monzogabbros (Fig. 6). Seven distinct volcanic breccia events are present, four of which are in the northeastern and three in the central portion of the complex. The trachyte, microsyenite, and bostonite dykes are also observed (Trein *et al.* 1967, Vasconcellos and Gomes 1992, 1998). The igneous breccia bodies are related to a variety of country rocks, such as phyllite clasts, syenites, and breccias, the latter formed from former breccia bodies (Baêta and Vasconcellos 2004). The features such as rectilinear scarps and captured river segments are in direct association with aeromagnetic and structural lineaments in the complex (Figs. 2, 4, 5, and 6), which are characteristic of morphotectonic processes and may indicate neoformation or reactivation faulting.

Successive deformational events were previously reported in the TAC, designated as A and B and identified by the presence of fractures along N-S to NNW-SSE and NW-SE directions. Their kinematic indicators point to two distinct deformation pulses with fractures oriented to 10° and 260° azimuths (Di Giorgio 2003).

In terms of geochronology, analyses confirmed that the complex was formed in the Upper Cretaceous (Gomes *et al.* 1987), with predominant K/Ar ages between 80 and 90 and Rb/Sr ages of 80.5 Ma. Siga Jr. *et al.* (2007) reported more precise thermal ionization mass spectrometry isotopic dilution (ID-TIMS) and sensitive high-resolution ion microprobe (SHRIMP) U-Pb ages between 82.7 and 84.7 Ma, using zircon crystals.

RESULTS

Remote sensing lineaments

The initial determination of brittle deformation in the TAC consisted of interpretation of the most prominent lineaments.

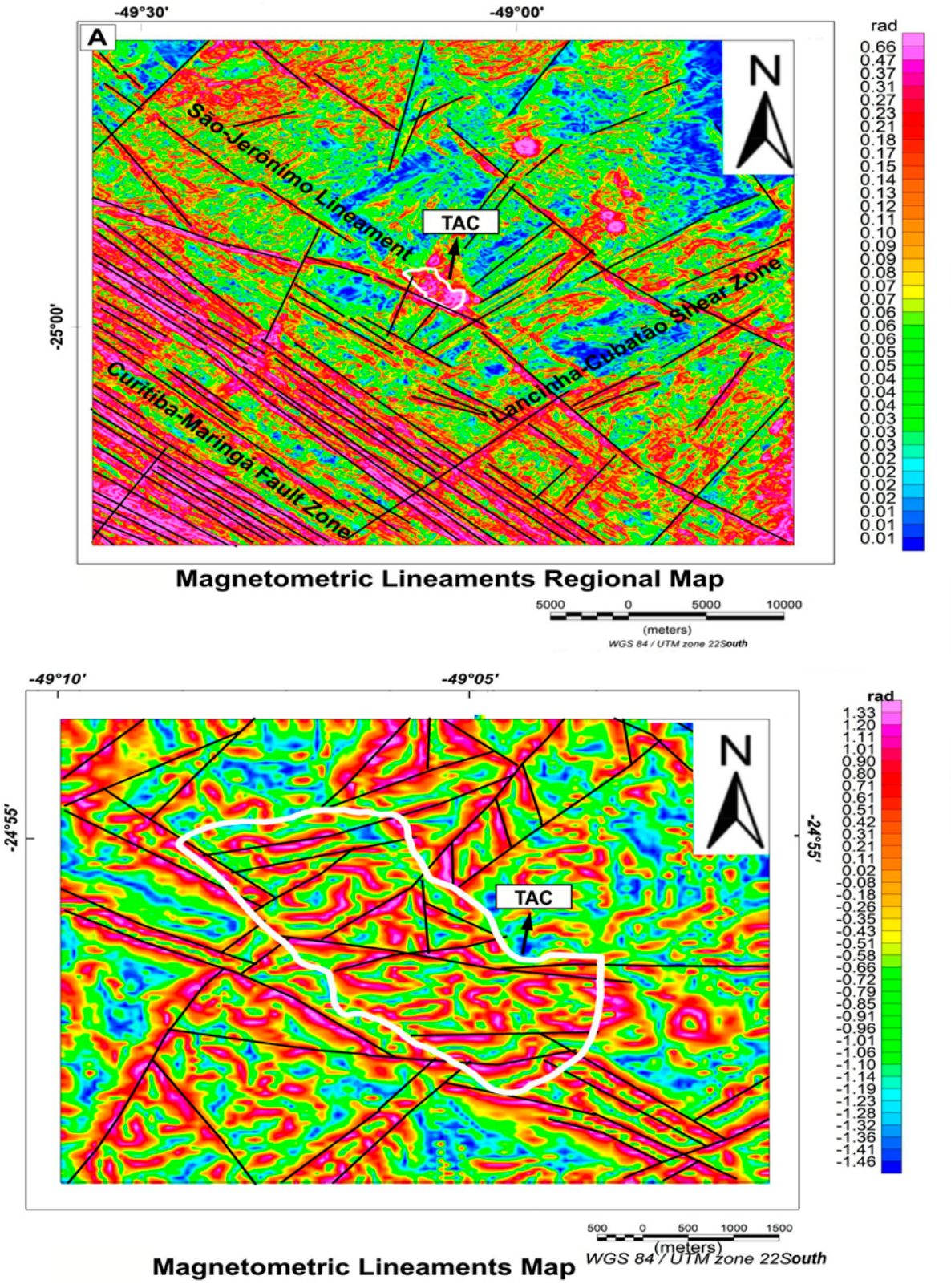

Figure 5. TAC's magnetometric lineament maps showing the Lancinha-Cubatão Shear Zone oriented in a N45-50E direction and the São Jerônimo-Curiúva Lineament oriented in a N45W direction: (A) regional THG magnetic interpretation map showing the TAC in the center of the map; (B) 1:50,000 ASI-THG magnetic interpretation map of the area. The white line outlines the boundary of the complex.

Figure 6 depicts our interpretation correlating it with the geological map of the area. The lineaments that adjusted most accurately to the field data were those interpreted in aerial photography with 1:70,000 scale. The azimuth-frequency rose diagram in Figure 7A reveals a predominantly NE-SW structural trend oriented to the N40-50E direction, followed by the N20-40E- and N80-90E-trending elements, with noticeable variation between ENE-WSW and WNW-ESE directions. In turn, the N-S-trending lineaments are less frequent, however, more extensive (longer than 2 km in length). In contrast,

the E-W to WNW-ESE- and NE-SW-trending structures were more prominently detected from ASI-THG aeromagnetic data (Fig. 5); Figure 7B also shows the NE-SW- and NW-SE-trending structures.

In the complex, the most frequent drainage trends are predominantly in a N20-30E direction and less frequently in N0-20E, N30-60E, and N40-70W directions (Fig. 7C). Drainage elements longer than 500 m, in turn, are oriented mainly in N30-70W, especially in the N50-60W and N0-50E directions, as well as in the N0-20E directions (Fig. 7D).

The southeastern border of the TAC is represented by a NW-SE-striking dextral fault that extends along elevations higher than 1,000 m and in the vicinities of this lineament, characterizing knickzones, in the sense of Crosby and Whipple

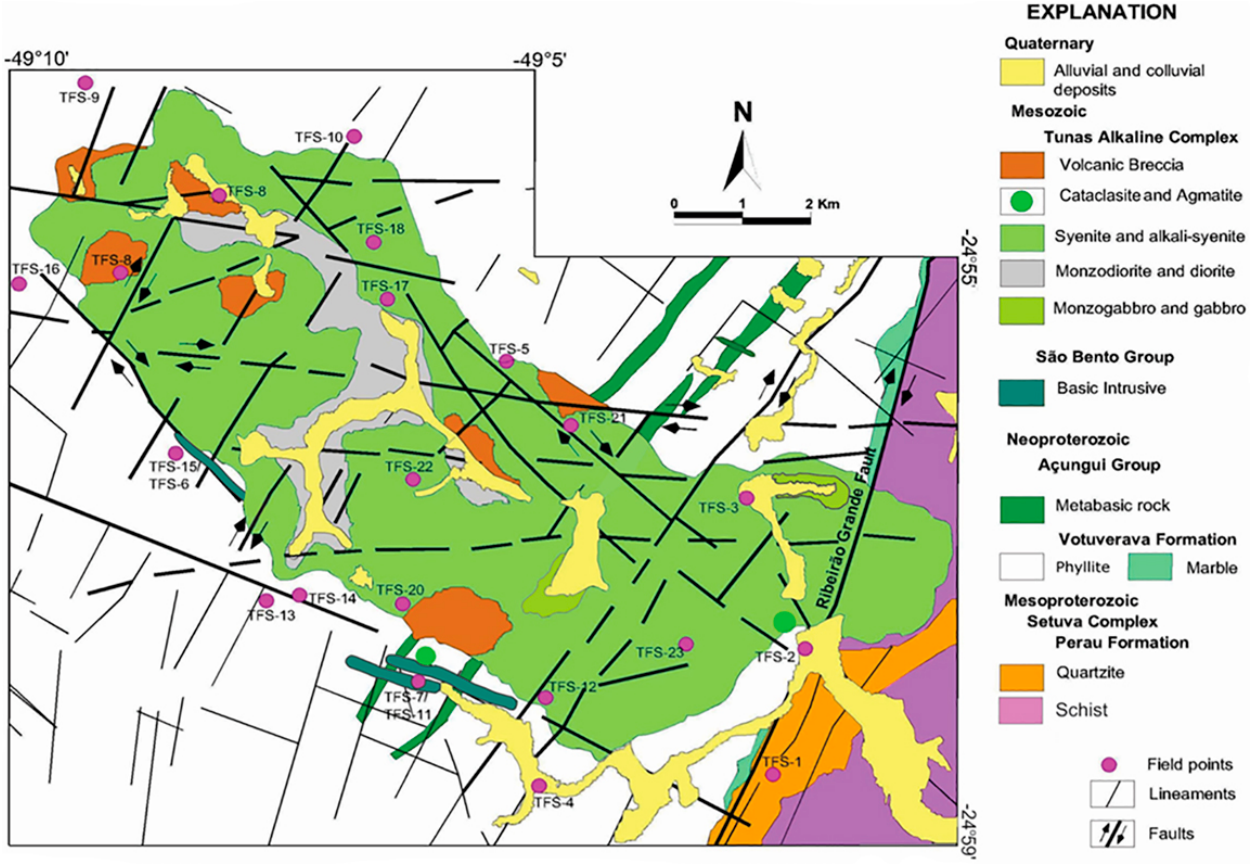

Source: geology map modified from Vasconcellos and Gomes (1992).

Figure 6. TAC's geological map representing faults and lineaments interpreted from ASTER-GDEM data.

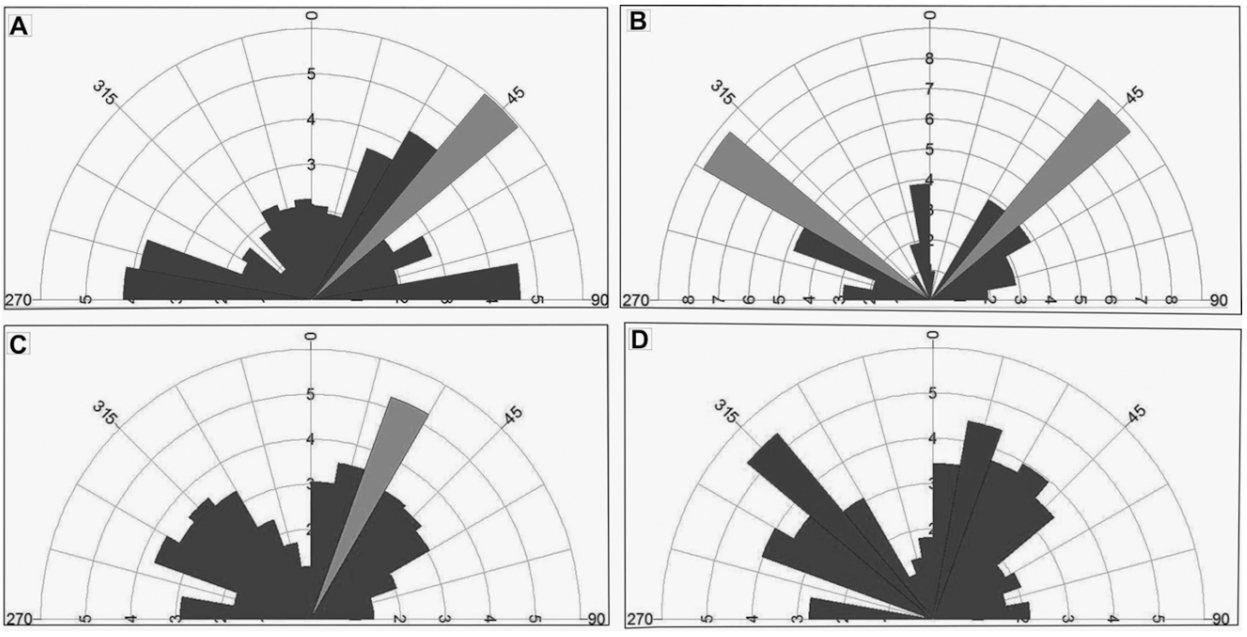

Figure 7. Rose diagrams for lineaments frequency: (A) photointerpreted lineaments, n = 336; (B) ASI-THG aeromagnetic lineaments, n = 52; (C) drainage lineaments, n = 638; (D) drainage lineaments longer than 500 m, n = 164. Highest occurrences are represented in light gray, followed by the lowest occurrences in dark gray.

(2006). The Gramado stream runs along the NE-SW direction and marks the southeastern border of the TAC, showing a scarp associated with the N10E fault direction (Fig. 2). The Ribeirão Grande river, in turn, oriented in the NNE-SSW direction, is partially captured by one of the complex's most extensive faults (Fig. 2). We can also observe an important E-W-trending lineament given by the São Domingos river.

Fault geometry and kinematics

The best exposed syenite and breccia events were found at stone quarries, where fault planes with good lateral continuity were observed, therefore favoring the collection of structural data.

Part of the oldest structures of the TAC were filled with trachyte dykes oriented to the N75E (Fig. 8A), N20E, and N50W directions and microsyenite dykes that were oriented in the N30E (Fig. 8B), NE-SW, N80E, and NW-SE directions.

The main fault systems in the TAC are oriented in the N50E and N30E trends; N20-30W and N45W; N20E-N20W; and N70-90E and N70-90W trends, as observed from the field data. The dextral strike-slip faults with high dip angle — many of them vertical and subvertical — are predominantly oriented in the NE-SW direction, especially to the N30-50E, N70-80E, and N70-80W trends and, secondarily, the N40-50W trends (Fig. 9A). The sinistral strike-slip faults, in turn, are mostly oriented in the N60-70E and N40-50E, N10-20W and N80-90W, and, less prominently, occur in the N0-10E, N50-60E, and N60-70W and N70-80W trends (Fig. 9B). The normal faults intersecting the complex are predominantly oriented in the N70-80E, N30-50E, and N70-80W, and, secondarily, in the N30-40W and N60-70W trends (Fig. 9C). A considerable amount of the described faults and joints are conjugate (Figs. 10A, 10C, and 10D).

Parts of the NE-SW-direction faults were filled with kaolinite and illite (Fig. 11), as determined by XRD (Suppl. Mat. 2) and, secondarily, they contain oxides (Fig. 10B), quartz, epidote, silexite, or dark gray amorphous silica (Fig. 10F). There are fillings of probable pseudotachylites or oxides which are present in the failure plans (Fig. 10G). Not rarely, fault planes show kinematic indicators such as R-fractures (Fig. 10B), sigmoids (Fig. 10G), and striae (Figs. 11 and 14).

The N50E-striking faults usually show decimetric damage zones, with generation of cataclasite, breccia, and microbreccia and impregnations of manganese oxide. The predominant kinematics of fault-slip is sinistral, with subsidiary dextral and normal faults. In turn, the N30E-striking dextral strike-slip faults cut NW-SE-direction faults, with apparent displacement of up to 500 m (as observed on 1:50,000 scale geological maps, Fig. 4). Locally, they form decimetric damage zones filled with iron or manganese oxides and the N60-70E-striking sinistral and the N60-80W-striking dextral strike-slip faults may occur as transtensional conjugate systems or negative flower structures (Fig. 12B). It must be stressed, however, that the N60-80W-striking faults present two displacement histories, namely, a sinistral and a subsequent dextral one.

Both normal and strike-slip faults show dip angles varying between 70° and 90°. The subhorizontal slickensides are marked on fibrous clay filling (Fig. 11B) and oblique to vertical slickensides often may coexist in the same fault plane (Figs. 11A and 11C).

Figure 12A shows a geometric profile view of flower structures related to the transtensional faults in the contact between metasedimentary rocks of the Votuverava Formation and the TAC. Such features result in the formation of faults with opposite dip directions. In the field, we observed oblique slickensides in the more conspicuous planes, with rakes of up to 50°. A second

Figure 8. Dykes: (A) ENE-WSW-trending trachyte dykes; (B) NE-SW-trending tectonically controlled trachyte dyke showing reactivation of country rock faults (TFS-23).

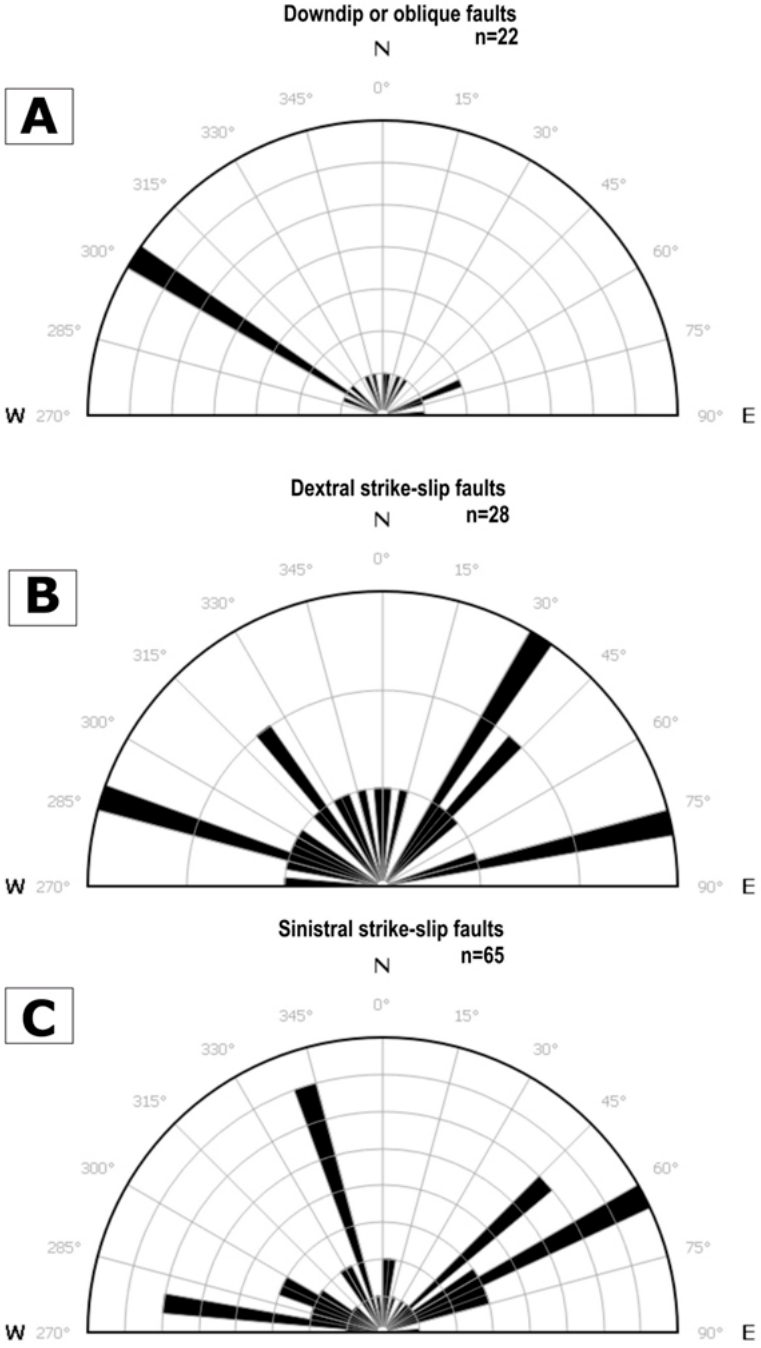

Figure 9. Rose diagrams of field fault data displaying the main direction trends of faults: (A) dextral strike-slip or transtensional faults, n = 27; (B) sinistral strike-slip or transtensional faults, n = 65; (C) medium to high dip normal (downdip or oblique) faults, n = 22.

configuration of flower structures is present, associated with N60-70E sinistral and N60-70W-striking dextral fault planes (Fig. 12B).

The fault system which resulted from strike-slip or transtensional tectonic regime is predominantly oriented in the N-S and NE-SW directions, being conjugated among them. Larger scale faults such as the sinistral N50E-striking faults show centimetric to decimetric fault-grinding breccia bands and associated gauge. In such cases, striae in the fault planes mark distinct dip angles that, together with steps, indicate sinistral kinematics. The fault surface is planar to rough, with damage zones identified by parallel fracturing and fine fault-grinding breccias. The flower structures formed by the N50E-striking faults are associated with the N20W-striking step faults and N30E-striking dextral cataclastic planes which characterize the structure's R'-shears in the fracturing model of Riedel and may be filled with kaolinite or illite. The dip angles of such structures are almost vertical, varying from 80 to 90°, with structures that resulted from reactivation of early sinistral faults. Locally, the N50E- and NE-striking faults show damage zones up to 1 m thick, with generation of gouge as well.

The deformation of the complex was also recorded as rhomboid fractures typical of brittle regimes (Fig. 10A), profile R-conjugated faults (Fig. 10B), faults in plain view (Fig. 10C), E-W-striking shear zones, and conjugate fractures (Fig. 10D),

Figure 10. Structural features observed in the field: (A) a rhombohedral pattern in conjugate faults under brittle deformation (TFS-08); (B) R-fault cross-sectional view filled with Fe and Mn oxides (TFS-022); (C) cross-sectional view of fault intersection (TFS-018); (D) cross-sectional view of the relationship between conjugate N70-80E- and N70-80W-striking faults associated with the main E-W-striking fault (TFS-022); (E) rectilinear contact between syenite and trachyte dyke (TFS-12); (F) fault gouge of the N50E-striking sinistral strike-slip fault plane filled with dark gray colored amorphous silica (TFS-021); (G) sigmoidal-shaped fault line (TFS-018) with sinistral strike-slip movement.

as well as rectilinear to curvilinear contact of microsyenite and trachyte dykes (Fig. 10E) trending in the N30E direction. Some open fractures present silexite filling associated with the N50E-striking fault zone (Fig. 10F). In addition, we described sinistral N50E-striking fault planes with R-conjugates (Fig. 10G), showing probable sigmoidal pseudotachylites (Fig. 10G); the cataclastic flux may also be represented, presenting a clay mineral rich matrix.

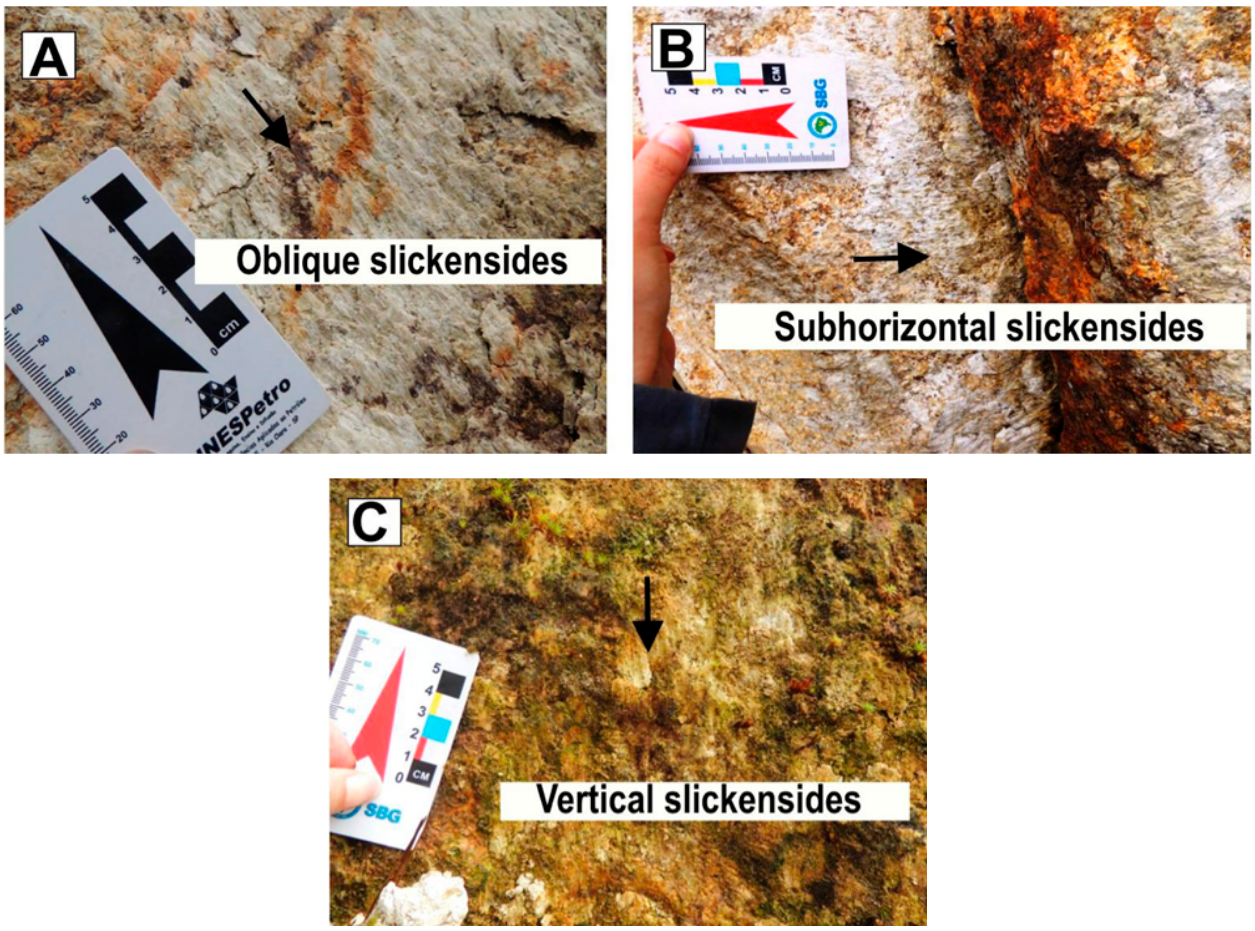

Figure 11. Fault slickensides on fibrous clay (TFS-012; see Fig. 6): (A) oblique; (B) subhorizontal; (C) vertical.

The NW-SE-striking fault planes are considerably uniform showing high, sometimes even vertical, dip angles. In the field, the NW-SE-striking fault partially marks the boundary between the complex and the metasedimentary rocks of the Açungui Group (Fig. 6). In satellite imagery, the NW-SE-trending fault determines the capture of rectilinear valleys and rivers. In the field these fault systems consist of three predominant directions, which are N20-30W, N45W and N70-80W-striking faults. The N30W-striking fault planes are smooth to rough, irregular, and show kinematics normally sinistral, while N70-80W-striking structures may be associated to decimetric horsetail and flower structures, both showing strong cataclasis and related breccias. The N45W-striking are frequently dextral strike-slip faults and are not very expressive, although they occur locally as flower structures or R'-shears related to the N60E-striking sinistral strike-slip planes (Y). In general, they are impregnated with Fe and Mn oxides, showing centimetric damage zones locally filled with quartz or striated fibrous clay, with horizontal rakes or dip angles of up to 50°. Also, they present strong cataclasis and breccia associated to centimetric to decimetric damage zones.

In the field, the fault system oriented approximately to NE-SW direction stands out as much as the N30E and N50E-striking planes, being exposed at nearly all outcrops visited and conditioning aligned rectilinear morphostructures (valleys and crests; Fig. 3).

In turn, the E-W-striking sinistral strike-slip faults precede the E-W-striking dextral strike-slip faults, as noticed from the superimposition of steps and striae. A relative chronological sequence was built based on deformation events that took place in the area. As in aforementioned structures, E-W- striking faults have high dip angles and have prevailing dextral kinematics, being recognized in the field by their extensive planes, as well as by curviplanar, rough and commonly open, striated carbonatic clays and associated microbreccias. Macroscopically, N70-85E- and N70-85W-striking faults frequently show cataclasis and normally present thick striated MnO_2 crusts, implying that the faults are relatively young.

The faults approximately oriented in the N-S direction are of subsidiary presence in the field, and their planes are often sigmoidal and metric, showing presence of striated carbonatic clay and steps that indicate sinistral kinematics. Between the N20E and N20W direction, high dip strike-slip fault planes were locally reactivated from ancient, centimetric trachyte veins. They present expressive cataclasis with fault breccia and centimetric to decimetric damage zones.

Figure 13 depicts other structural features of the TAC, such as the association of breccias and conjugate faults and associated sinistral displacement (Fig. 13A), crescent marks that correspond to sinistral strike-slip faults (Fig. 13B), conjugate faults (Fig. 13C), and curviplanar N-S-striking faults

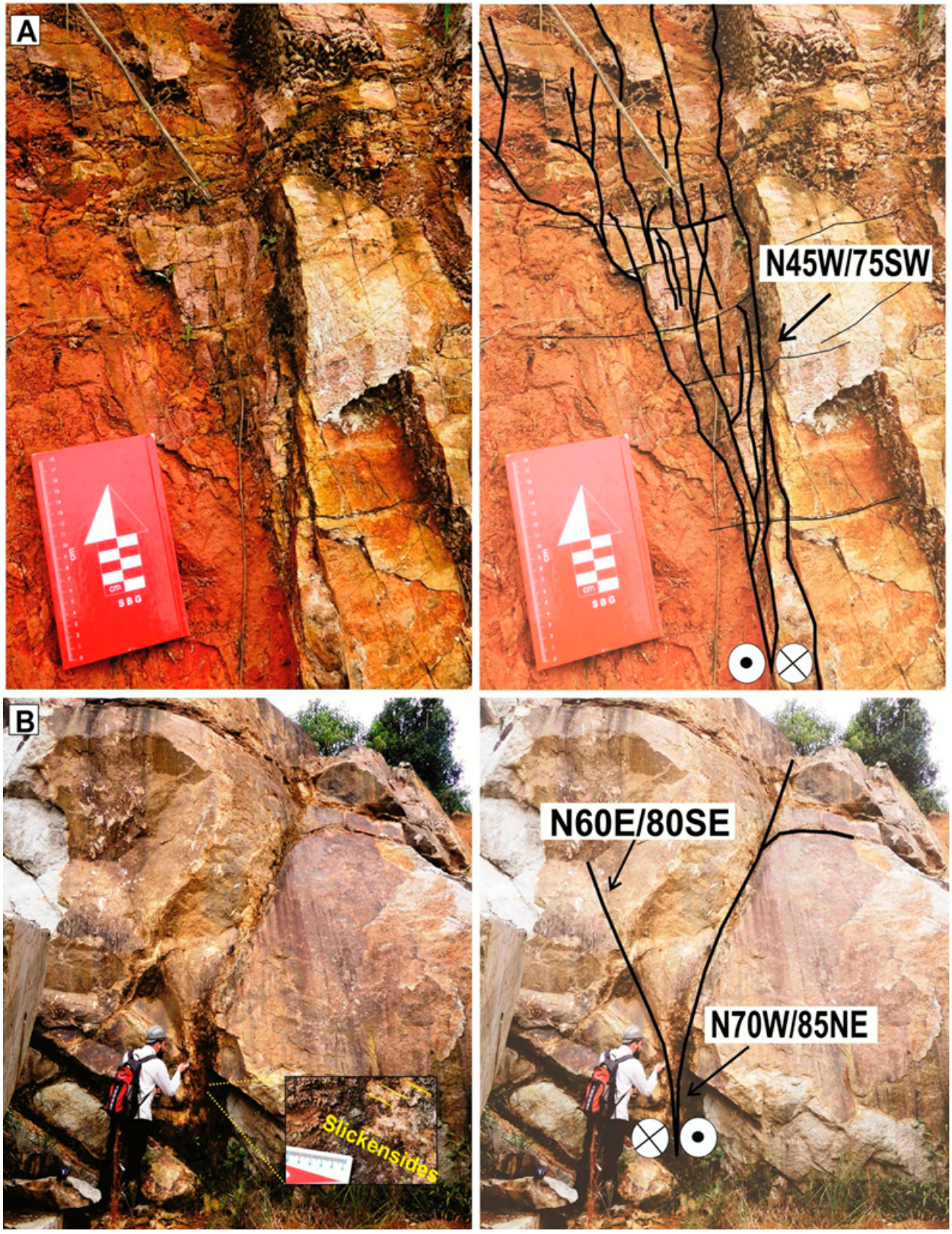

Figure 12. Flower structure sections: (A) negative flower structures at the contact between TAC and Votuverava Formation country rocks (TFS-01). The structure is associated with a N45W-striking sinistral strike-slip fault (Fig. 6); (B) negative flower structure in the TAC with complementary angles of about 60º (TFS-12), associated with an approximately E-W-striking dextral shear zone.

with heterogeneous deformation and the generation of breccias (Fig. 13D).

Slickensides normally affect recrystallized oxides or clay content filling fault planes. Also, the striae found at the N50-60E-striking fault planes (Fig. 11) show subtle repetition at the microscopic scale, as in 75x, 200x, and 500x (Fig. 14). In addition to striae, secondary structures such as steps formed by mineral growth, spoon-shaped sink structures and synthetic (R) and antithetic (R')-shear fractures are also common.

Figure 15 is a scheme illustrating the main average fault orientations and their cross-cutting relationships:

- NE-SW-trending paleostress field associated with the N20E-striking dextral and N40E-striking sinistral conjugated faults and N80W-striking sinistral fault dislocates a N-S-trending trachyte dyke (Fig. 15A);
- NNW-SSE-trending paleostress field that reactivates the N40E-striking sinistral fault that offsets a N40W-striking dextral that, in turn, dislocates the N70-80W-strike-slip faults (Fig. 15B);
- NW-SE-trending paleostress field related to N80W-striking dextral faults that were originally sinistral, now reactivated with dextral kinematics and occurring in association with the N20W-striking sinistral faults (Fig. 15C).

Based on total structural records seen in the field, four paleostress fields were evidenced (Fig. 16) deforming the TAC:

i. the NW-SE (σ_3) extension with vertical (σ_1) stress field and reactivation of the normal N50E- and N60-80E-striking faults from basement structures (preferential orientations of Proterozoic foliation);
ii. the NE-SW to ENE-WSW (σ_1) compression that reactivated N30E-striking dextral faults and the N70-80W-striking sinistral faults;
iii. an approximately NNW-SSE (σ_1) compression that reactivates early dextral N40-60E-striking faults as sinistral faults and early sinistral N40-60W- and N70-80W-striking faults as dextral faults;
iv. a WNW-ESE compression that reactivates the sinistral N70-80E-striking faults as dextral and the early dextral N20-30W-striking faults as sinistral faults. The N70-80E-striking sinistral faults are associated with negative flower structures. When this paleostress field varies approximately in the E-W direction, it might activate the N30-40E-striking dextral faults.

DISCUSSION

The research was based on the geometric and kinematic structural analysis of faults that intersect the TAC. The paleostress fields revealed by the geometric and kinematic analysis of these faults delimit at least four tectonic pulses (I, II, III, and IV). In addition, the description of the faults allowed

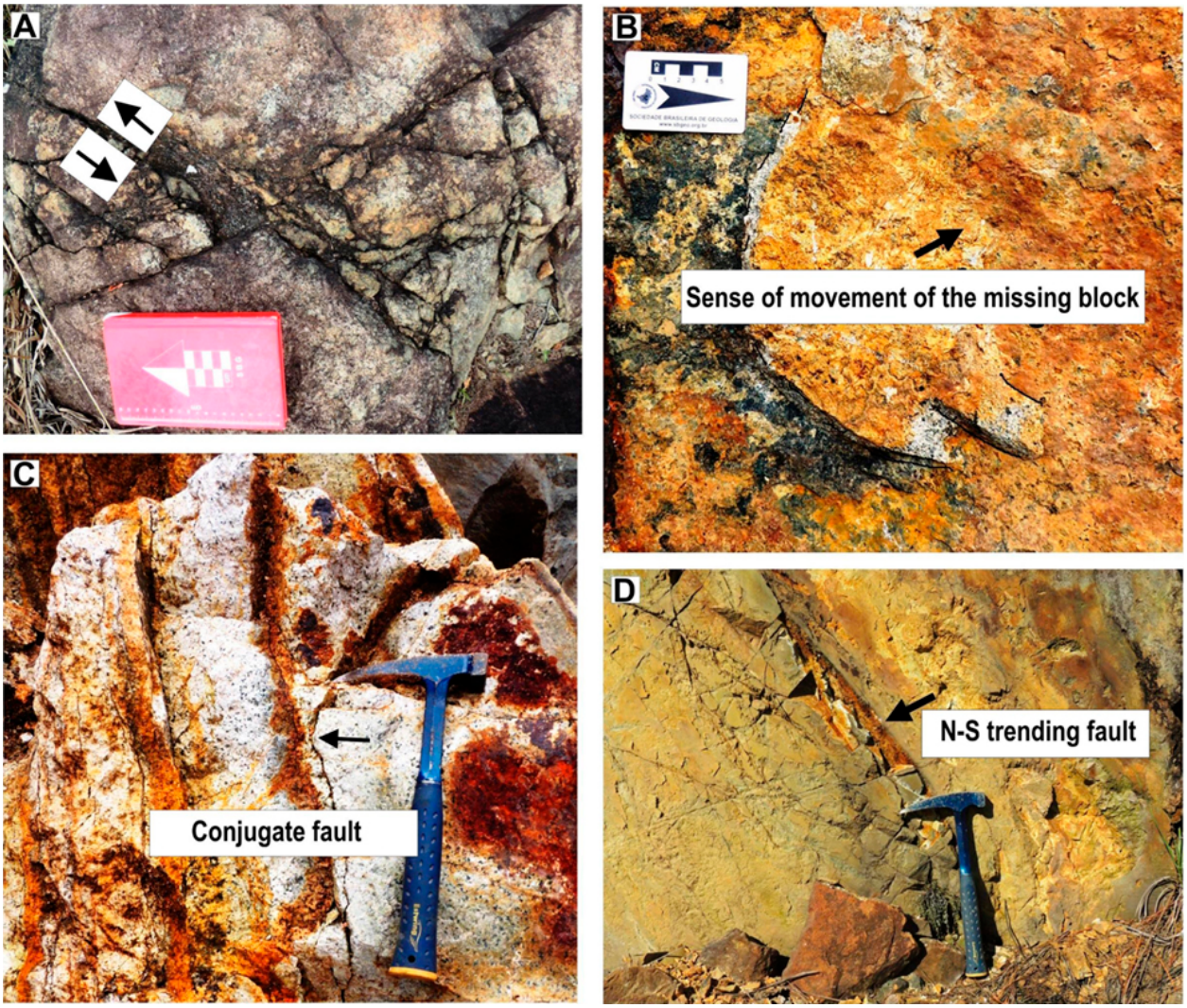

Figure 13. Structural features of the TAC: (A) Plan view of associated breccia in sinistral conjugate faults (TFS-17); (B) crescent mark typical of sinistral displacement of missing block (TFS-18); (C) profile view of conjugate N40W and N-S-striking fractures (TFS-12); (D) curviplanar N-S-striking fault with adjacent blocks showing heterogeneous deformation (TFS-08).

the development of a Cenozoic brittle tectonic model for the complex, comprising the central region of the Ponta Grossa Arch, especially the Curitiba-Maringá Fault Zone, located between the São Jerônimo-Curiúva and Rio Alonzo Lineaments (Figs. 4 and 5).

We consider that the regional brittle tectonism was a consequence of the tectonic processes initiated in the end of the Cretaceous period, and the proposed model was compared to similar studies in southern and southeastern Brazil. Our research provides an important source of discussion regarding Cenozoic tectonics in the context of the intraplate deformation between southern and southeastern Brazil and may also be applied to studies of mineral prospecting, as well as to groundwater and oil and gas research in the offshore arc domain.

To comprehend the chronology of such events, a hierarchization was established based on macrostructures photointerpreted from orbital products (Figs. 2, 5, and 6), structural aspects in the field (Figs. 8, 10, 11, 12 and 13), and field intersection of faults, while stress fields were obtained from geometric relations and kinematic indicators of faults (Figs. 10, 11, 12, 13 and 15).

The thermochronological studies evidenced at least two cooling events in the development of the morphotectonic framework of southeastern Brazil (Modica and Brush 2004, Siqueira-Ribeiro *et al*. 2012, Cogné *et al*. 2011). The paleostress fields corresponding to the tectonic pulses (A to D frames, Figs. 16 and 17) were correlated, in part, to the data from AFT analysis (Fig. 18). Data of the Serra do Mar in São Paulo indicated that tectonic pulses took place in the Upper Cretaceous (~80 Ma), Paleocene (~60 Ma), Eocene (~40 Ma), Oligocene (~25 Ma), and Miocene (~10 Ma) (Hadler *et al*. 2001). A tectonic pulse aged 16.95 ± 1.05 Ma also took place between the São Jerônimo-Curiúva and Rio Alonzo Faults (Franco-Magalhães *et al*. 2010b).

The geometric and kinematic analyses were performed in order to identify the paleostress fields responsible for the brittle structures and, after analyzing the results, to interpret the relative chronology of the deformation pulses that affected the complex. The different geometries of fault families require a superimposition of deformation events that nucleated new faults and reactivated older ones in the country rocks. It is worth highlighting that the TAC's conduits are shallow, one of them being 3 km deep as determined from aeromagnetic data (Rugenski 2006). It means that the reactivation of faults that were older than the complex was marked by the presence of breccias and fault gouge associated to the N40-50E-striking sinistral fault.

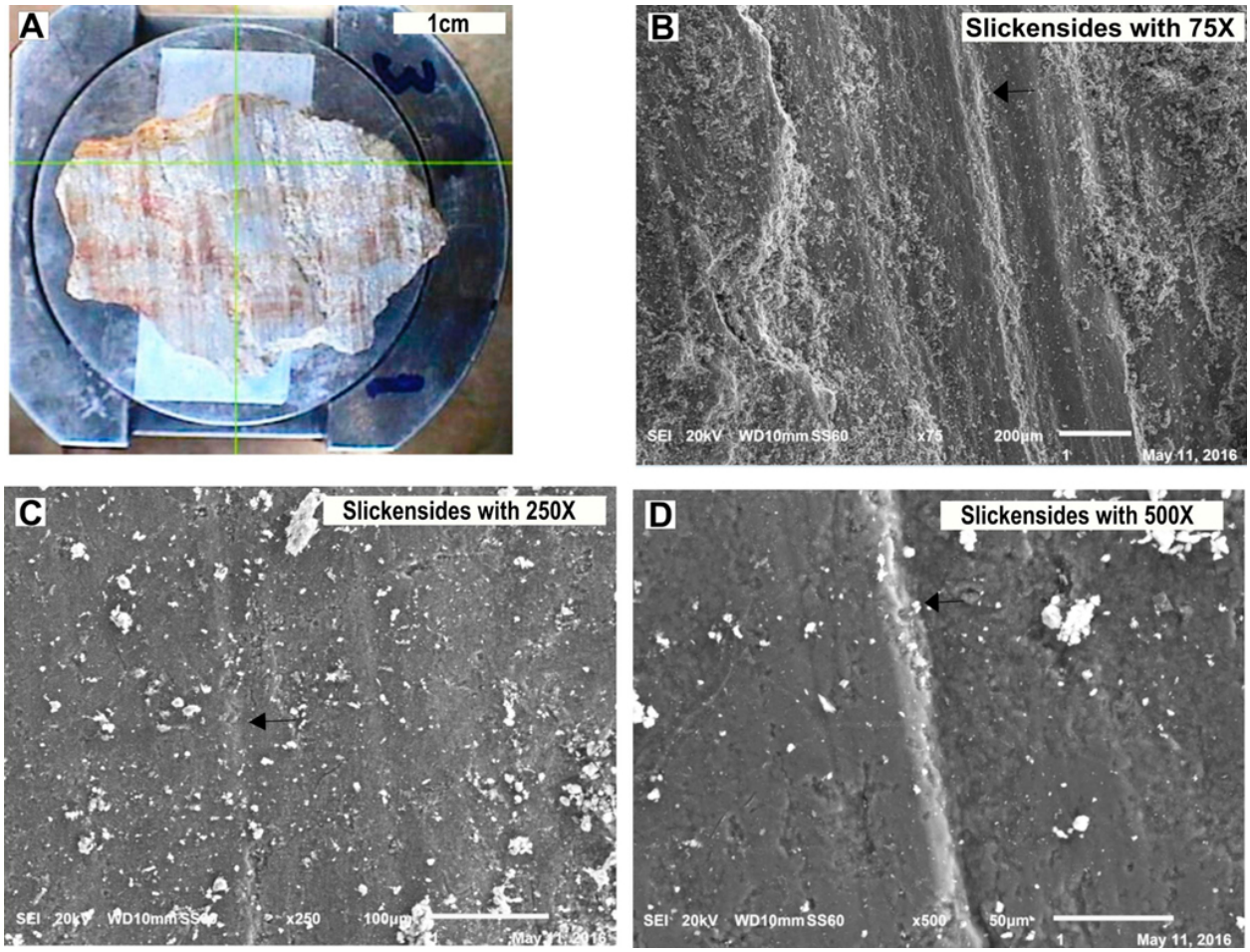

Figure 14. Scanning electron microscope (SEM images) of striae. Images registered of SEM with N50-60E-striking fault plane striae at different scales (TFS-12): (A) centimetric striae on kaolinite and illite; (B) rectilinear features represented by 75× (200 micra); (C) striae represented by 250× (100 micra) rectilinear features; (D) rectilinear features represented by 500× (50 micra); striae can be noticed despite the subtleness of the feature.

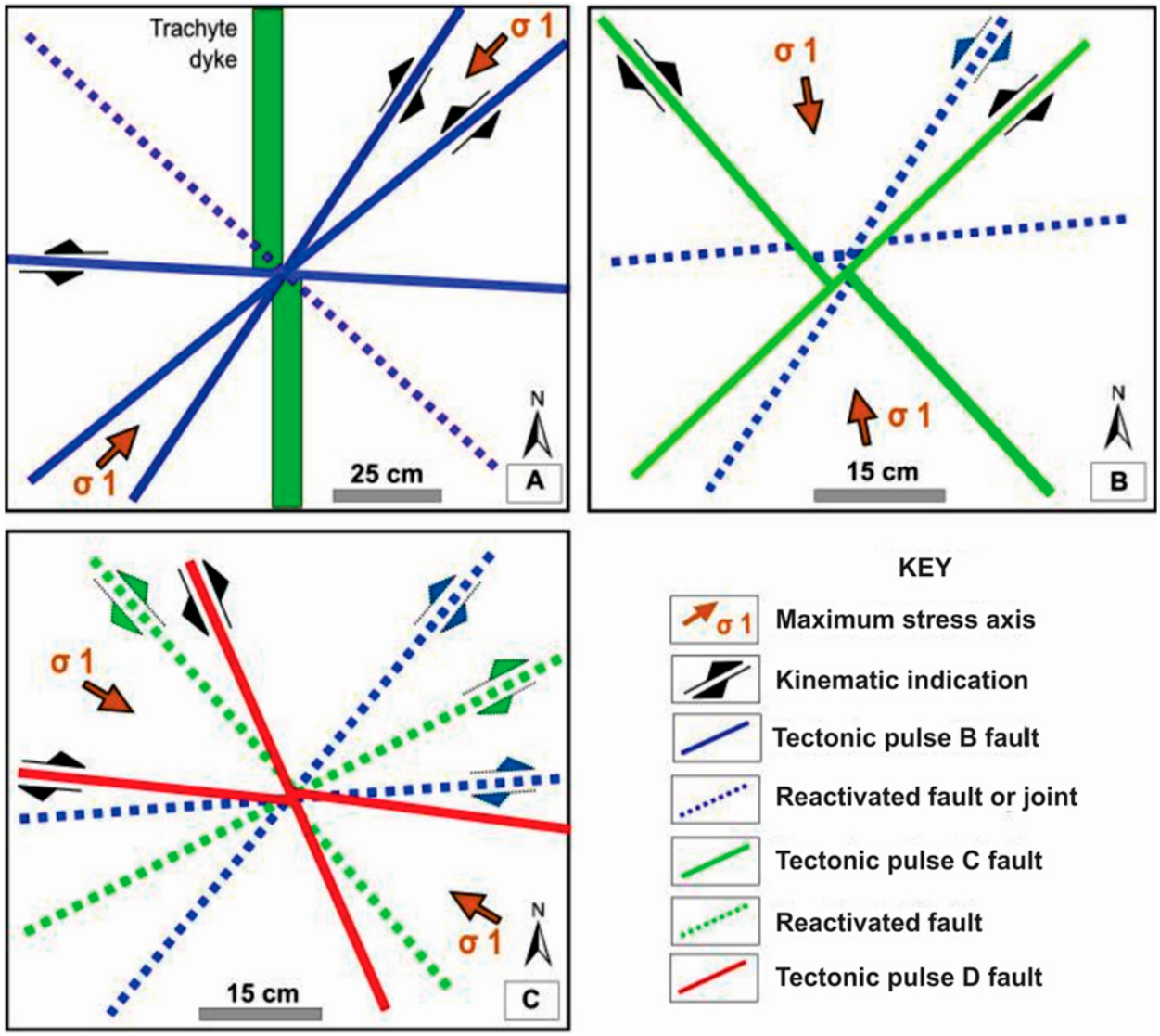

Figure 15. Intersection between the strike-slip faults in the TAC: (A) NE-SW-trending paleostress field associated with the N20E-striking dextral and N40E-striking sinistral conjugated faults and N80W-striking sinistral fault; (B) NNW-SSE-trending paleostress field related to N50E-striking sinistral and N40W-striking dextral faults; (C) NW-SE- to WNW-ESE-trending paleostress field related to N20W-striking sinistral and N80W-striking dextral faults.

In the northwest of TAC, the E-W-trending lineament of the São Domingos river (Fig. 2), generated by the NE-SW (σ_1) compression (tectonic pulse II), was interpreted as a fault displaced by subsequent NW-SE-striking dextral reactivation (σ_1 ~NNW-SSE; tectonic pulse III).

The N70-80E- and N70-85W-striking faults developed from the reactivation of ancient structures filled with epidote and potassium feldspar or amphibole (forming the structural flowers related to the tectonic pulse IV).

Part of the TAC's faults were filled by trachyte and microsyenite dykes (the NE-SW-, N80E-, and NW-SE-striking faults), while N75-85E- (Fig. 8A), N20E-, and N50W-striking faults were filled by trachyte. We consider them to have been emplaced after the microsyenite bodies, given their shallower crustal levels and the presence of bostonite dykes oriented N-S, which were also observed by Fuck (1972). Some dykes are present where fracture density is higher, possibly marking reactivated deformation corridors (Almeida *et al.* 2013). In TAC, a preferential trachyte dyke trend in the N30E direction was observed (Figs. 8B and 10E) and interpreted as a result of basement fault reactivation along Ribeirão Grande Fault (N30E-striking fault; Fiori *et al.* 1998).

The negative N45W-striking flower structures were related to the intrusion of the TAC, marking the contact between phyllites of the Ribeira Belt and alkaline rocks of TAC. The four post-Cretaceous tectonic pulses (I, II, III, and IV) identified in this research correspond to those found in areas of similar age, such as the Rio Paraíba do Sul Shear Zone (Silva and Mello 2011) or in Paleogene basins (Riccomini *et al.* 1989, Riccomini *et al.* 2004, Salamuni *et al.* 2004) and post-Cretaceous activity in alkaline massifs (Chiessi and Riccomini 2003, Machado *et al.* 2012).

Therefore, while the N-S (σ_1) stress field (tectonic pulse III) formed or reactivated the N30E- to N50E-striking faults with sinistral kinematics, the WNW-ESE (σ_1) stress field (tectonic pulse IV) reactivated these faults as dextral ones. The field

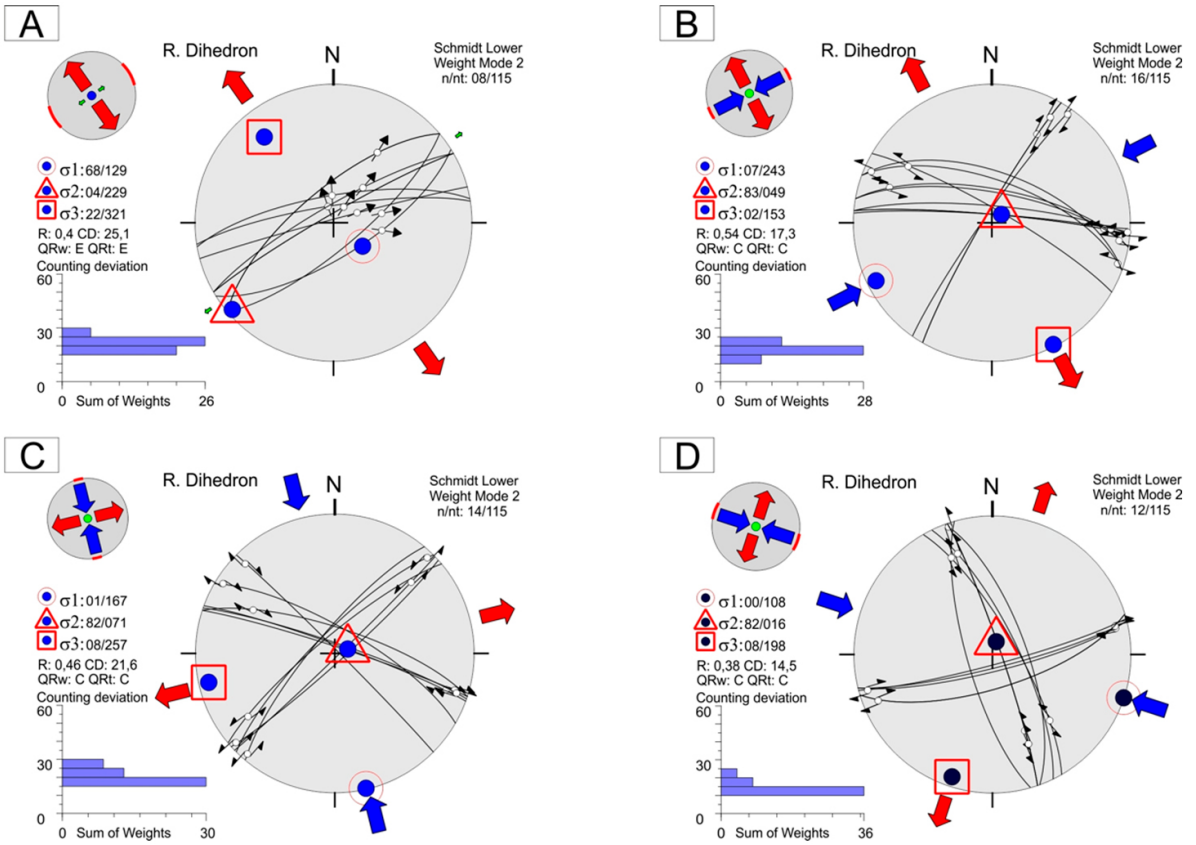

Figure 16. Paleostress diagrams of faults that affected the TAC: (A) NW-SE (σ_3) extension (tectonic pulse I) with vertical (σ_1) stress field and reactivation of the NE-SW normal faults; (B) NE-SW to ENE-WSW (σ_1) compression that reactivated NE-SW dextral faults and the WNW-ENEW sinistral faults; (C) the NNW-SSE (σ_1) compression associated with the NE-SW sinistral faults, NW-SE and WNW-ESE dextral faults; (D) the WNW-ESE (σ_1) compression associated with the NE-SW dextral faults and NW-SE sinistral faults. Maximum stress axes (σ_1) are represented as circles, while intermediate (σ_2) and minimum (σ_3) axes are marked as triangles and squares, respectively.

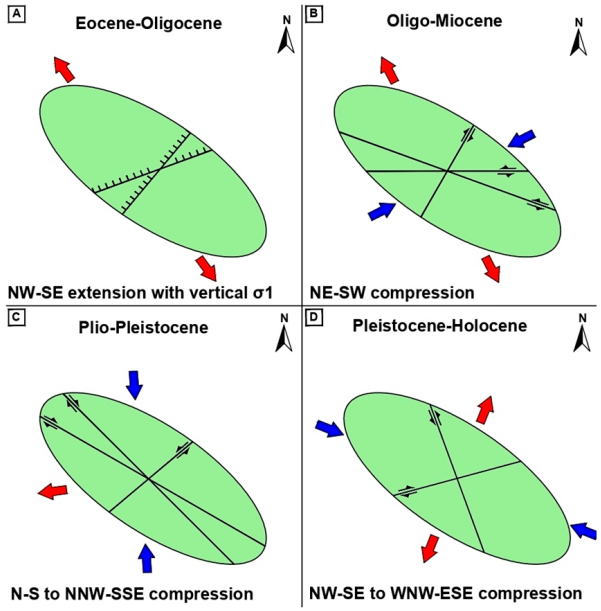

Figure 17. Proposed relative order of paleostress events for the TAC showing (σ_1) paleostress field (blue), (σ_3) paleostress field (red), mean orientation of the most important faults (black) from the synthesis of Figure 15 (field drawings), and the interpretation of the stereograms of Figure 16. The relative deformation sequence is given by: Eocene-Oligocene (σ_3) NW-SE extension (tectonic pulse I); (B) (σ_1) NE-SW compression with WNW-ESE-trending sinistral binary (tectonic pulse II); (C) Plio-Pleistocene (σ_1) N-S to NNW-SSE compression (tectonic pulse III); (D) Pleistocene-Holocene (σ_1) NW-SE to WNW-ESE compression (tectonic pulse IV).

observations allowed the estimation of the stress state compatible with the observed fault characteristics. In this case, brittle structures were considered to be fractal, the deformation persisting across different observation scales. A similar perspective was reported by Salazar-Mora *et al.* (2013) in Camburu Shear Zone (in the Ribeira Belt), where repetition of features occurs as both mesoscopic and microscopic scales of analysis.

The approximately E-W current stress (σ_1) to which the plate is submitted, in reality a variable stress field (σ_1) between WNW-ESE and NW-SE directions (tectonic pulse IV), could explain the morphotectonic accommodation of morphostructural segments (Fig. 2).

The extensive lineaments identified in regional analysis often repeat themselves in mesoscopic analysis of the complex (Figs. 4, 5, 6, and 15), with the more frequent orientations being in the N20-30W, N20-30E, N70-80E, N70-80W, and N40-50W directions. The NW-SE and NE-SW orientations correspond to preexisting country rock faults reactivated by new stress fields (σ_1), as the N45W and N60W trends are extensions of the São Jerônimo-Curiúva Lineament and the N30E and N50E trends are being related to the Lancinha Strike-Slip System (Fiori 1994).

From a morphostructural standpoint, the river segments longer than 500 m are aligned to the N40-50W-, N10-20E-, and N30-40E-trending lineaments, which correspond to the most extensive lineaments in the TAC. The N10-20E- and

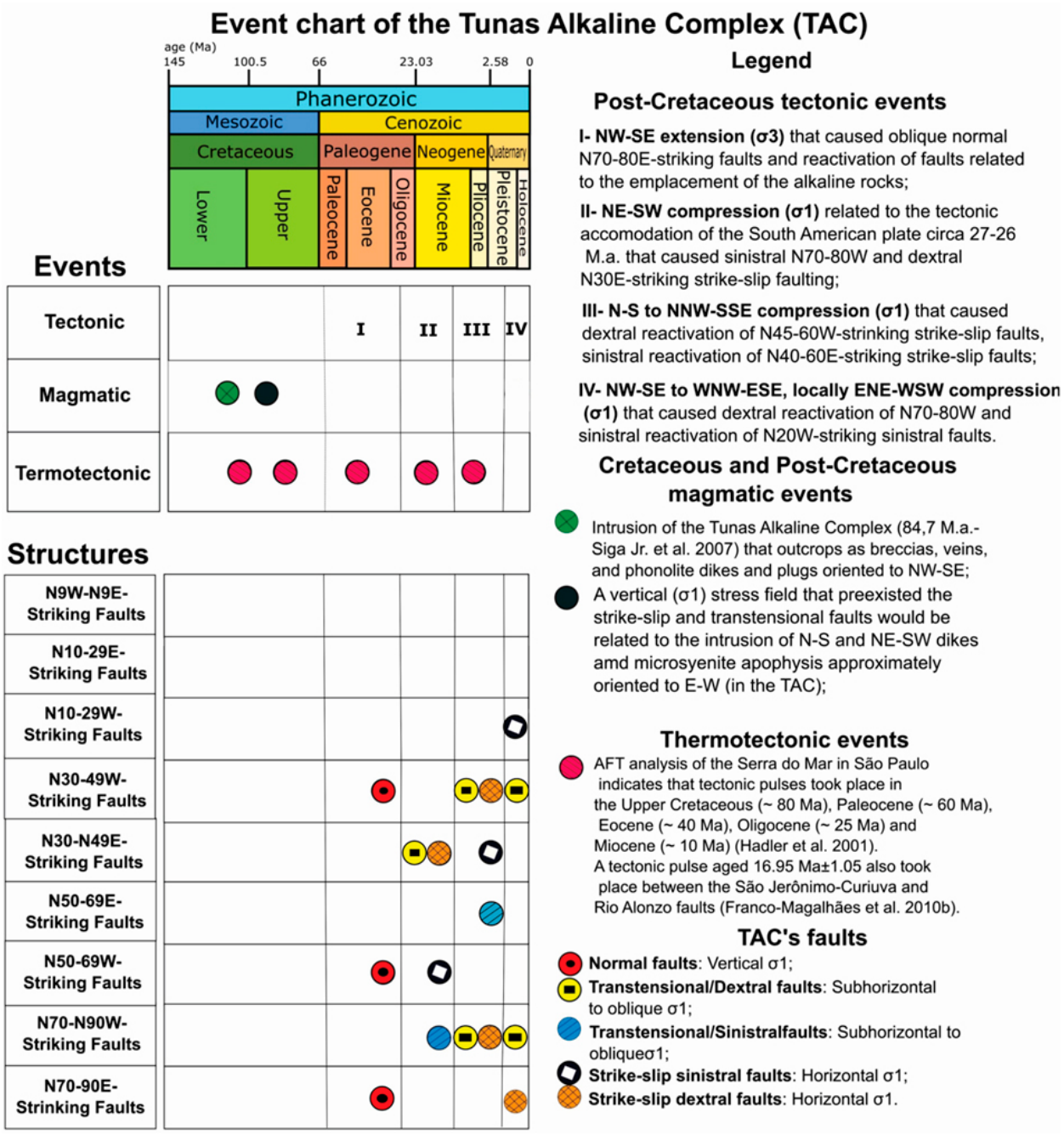

Figure 18. TAC event chart showing the main magmatic, tectonic, and thermotectonic events (given by Apatite Fission Track data) and their relationship with formed structures and consequent tectonic pulses.

N60-70W-striking faults are of limited expression in the surroundings of the massif, being interpreted as newly formed structures developed after the intrusion of the complex. In turn, the N40-50W-striking structures predominantly correspond to normal or dextral strike-slip faults, while the N10E-striking faults are generally associated to sinistral strike-slip faults. The ASI-THG and photointerpreted lineaments reveal marked presence of the N40-50E-striking structures associated with both dextral and sinistral strike-slip faults and, secondarily, to normal faults. This corroborates with the hypothesis that normal, dextral, and sinistral faults control the overall morphostructures of the complex, which allows us to interpret that the last tectonic pulse is active in the region as a transtensional event, which also relates to the generation of negative flower structures in the area (Fig. 12A).

The most frequent morphostructures aligned to the N20-30E direction (Fig. 7C) were interpreted as being resulted from a recent activity. In the country rocks of the complex, basic dykes are oriented to the N30E direction, the same direction as the trachyte dykes emplaced after the intrusion of the complex. These structures were affected by a deformation pulse that generated cataclasis associated with shear joint pairs, which may indicate recent reactivation of structural weakness planes.

In TAC, faults are predominantly directional, being mostly strike-slip and secondarily transtensional tectonic regimes. Their cross-cutting relations contributed to the understanding of the relative paleostress field chronology. These relations indicate that two distinct orientations of paleostress field were present at the same point in the field. Therefore, two distinct

stress adjustment patterns can correspond to generated or reactivated structures. It is worth pointing out that the same structure can behave as either a Y or R'-shear fracture, for example, depending on how (σ_1) stress was oriented during its generation.

This study was focused on Paleogene and younger directional structures; however, a vertical (σ_1) paleostress field prior to the strike-slip and transtensional faults is related to the intrusion of the N-S- and NE-SW-striking dykes and microsyenite apophysis, oriented to the E-W direction. Given the cross-cutting relations among all these structures, this deformational event is considered to have taken place prior to the aforementioned pulses, being related to Late Cretaceous tectonic pulses (Gomes *et al*. 1987, Siga Jr *et al*. 2007), but also being younger than those of the alkaline magmatism in Paraguay (Velázquez *et al*. 2011).

The brittle structures of the TAC were classified into fault systems, and a relative chronological order of lineament nucleation was established from field observation of their superimposition relations and the analysis of lineaments obtained from orbital products. For example, the N50E-striking sinistral faults reactivated or formed during a tectonic pulse with (σ_1) stress field were approximately along the N-S direction (tectonic pulse III) displaced the N30E-striking trachyte dykes and N-S-striking amphibolite veins, which confirm that the sinistral movement is subsequent to the magmatic history of the complex. Later, the N50E-striking sinistral faults were displaced by the N-S-striking faults, nucleated or reactivated with the (σ_1) stress field, which was oriented approximately to the NNW-SSE direction. It can be concluded, therefore, that the N-S compression direction is posterior to the tectonic pulse with (σ_1) stress better adjusted to the NE-SW (σ_1) stress (tectonic pulse II). The carbonatitic-alkaline complex of Mato Preto and the plug of Barra do Teixeira (Comin-Chiaramonti *et al*. 2001) testify that the reactivation of the NW-SE-trending structures was associated with the São Jerônimo-Curiúva Lineament being microsyenite and trachyte dykes. A similar record of extension was observed in dykes of the TAC, rarely presenting shear joints.

It can be observed from the field data that a post-Cretaceous deformation pulse identified by the NNW-SSE (σ_3) extension with (σ_1) was subvertical and reactivated or nucleated the N50E- and N70-80E-striking faults as normal was active in the TAC (tectonic pulse I; Figs. 16A and 17A). This deformation pulse would have remained active between Lower Eocene and Upper Oligocene, as evidenced by basic dykes of the Ponta Grossa Arch, by granites occurring at the Serra do Mar in the State of São Paulo, and by regional AFT analyses and synthesis (Hadler *et al*. 2001, Souza *et al*. 2008, Franco-Magalhães *et al*. 2010a, 2010b, Engelmann de Oliveira *et al*. 2018). Also, early in the Paleogene, between 65 and 54 Ma, an extensional tectonic pulse caused deformation of the Cananéia (Riccomini 1995), Passa Quatro (Chiessi and Riccomini 2003), and Domo de Lages (Machado *et al*. 2012) alkaline massifs. Further evidence was found in the Paraíba do Sul Shear Zone (Salvador and Riccomini 1995, Riccomini *et al*. 2004) and Lagoa de Araruama-RJ (Souza 2011).

A second tectonic pulse (II) that affected the TAC was interpreted as a NE-SW to ENE-WSW (σ_1) compressive field that caused dextral reactivation of the N30E-striking faults and generation of the N70-90W-striking sinistral faults (tectonic pulse II; Figs. 16B and 17B). For this pulse, a paleostress adjustment was applied, considering Riedel second-order fracturing, with the E-W-striking sinistral faults corresponding to a Y-binary, the N30E-striking dextral faults corresponding to R'-shear fractures, and the N70E-striking sinistral faults corresponding to R-shear fractures. We consider the NE-SW to ENE-WSW (σ_1) paleostress field to have remained active between Oligocene and Miocene, as in the Passa Quatro Alkaline Massif (Chiessi and Riccomini 2003) and other areas relatively near the TAC (Souza 2011, Machado *et al*. 2012, Peyerl *et al*. 2018). Alternatively, this deformation pulse might be considered to have started in the Lower Oligocene, given that AFT data yield deformation ages between 40 (Hadler *et al*. 2001) and 35 Ma (Souza 2008).

The third deformation pulse, defined by a NNW-SSE (σ_1) paleostress field (tectonic pulse III; Figs. 16C and 17C), was also recorded in the Atuba Complex and Guabirotuba Formation, located immediately to the southeast of the TAC (Chavez-Kus and Salamuni 2008). This pulse, which is of Neogenic age (Plio-Pleistocene), was responsible for the reactivation of the N40-60E-striking sinistral (R'-shear fracture) basement structures and N40-65W-striking dextral faults, as Y-shear fractures are present. The deformation was responsible for the development of negative flower structures and fluid percolation in the area. The NE-SW-striking planes are frequently striated and normally filled with kaolinite, recrystallized quartz, and, locally, illite.

A fourth deformation pulse was determined through field observation by the N70-80W-striking transtensional/dextral strike-slip faults and the N20W-striking transtensional/sinistral strike-slip faults developed under (σ_1) paleostress field oriented to approximately between NW-SE and WNW-ESE trend (tectonic pulse IV; Figs. 16D and 17D). Such behavior, also observed in the Campos do Jordão Plateau and along Serra do Mar (Hiruma *et al*. 2001, 2010), was responsible for the reactivation of basement faults oriented to NE-SW- and ENE-WSW-striking faults (Cobbold *et al*. 2001, Souza *et al*. 2008, Cogné *et al*. 2011) under a directional tectonic regime related to AFT cooling data (Engelmann de Oliveira *et al*. 2018).

As in the aforementioned deformation pulses, an adjustment was made to second-order deformation, by considering that the N-S- to NNW-SSE-striking transtensional/sinistral strike-slip faults displaced the WNW-ESE-trending transtensional/dextral strike-slip faults, while the N55E-striking transtensional/sinistral strike-slip faults displaced the N30E-striking transtensional/dextral strike-slip faults. If the deformation involves (σ_1) the local variation of the stress field, which is probably the case, the WNW-ESE directional faults become sinister when the compression (σ1) directed to WNW-ESE (tectonic pulse IV) eventually migrates to the direction ENE-WSW. That explains the presence of both sinistral and dextral directional fault planes with striated kaolinite and illite, configuring the

most recent deformation registered in the TAC. In the field, as mentioned, slickensides with rakes varying from horizontal to steep (Fig. 11) indicate downdip displacement, pointing out to the presence of a relief component that caused transtension to be associated with a strike-slip regime.

The configuration of the fourth deformation pulse (tectonic pulse IV) is identified by the existence of a variable stress field (σ_1) between the NW-SE and WNW-ESE directions, which explains the displacement of the N30E-striking dextral faults, N70-80E-striking dextral, and N50-70W-striking sinistral faults. A dynamic structural analysis allowed us to interpret a small (σ_1) stress direction variation that would correspond to different deformation events in a single deformation pulse. The N70-80E- and N70-80W-striking faults, as well as the N30E-striking dextral ones are also filled with illite, calcite, and kaolinite, with slickenside and steps indicating both dextral and sinistral movements. This fact corroborates with the idea of relatively recent deformation, given the presence of unaltered clay mineral. In the brittle tectonic framework of the TAC, such deformation corresponds to the last tectonic pulse, which probably remains active. Nonetheless, a regional stress with current (σ_1) oriented in the E-W direction was admitted in the plate, based on geophysical studies (Assumpção *et al*. 2004, Assumpção *et al*. 2016). Other studies also evidence this regional compression direction as corresponding to a (σ_1) NW-SE to E-W stress field active from Upper Pleistocene to Holocene (Riccomini 1995, Salvador and Riccomini 1995, Hiruma *et al*. 2001, Salamuni *et al*. 2004, Souza *et al*. 2008, Silva and Mello 2011, Moura and Riccomini 2017).

Figure 17 shows a proposal of a chronological order of deformation events in the TAC. In the wider regional perspective, the extensional pulse (tectonic pulse I; Fig. 17A), with (σ_1) vertical, was well identified in previous thermochronological studies, being related to a brief heating episode followed by a long cooling period due to the Eocene-Oligocene reactivation of the NE-W- and ENE-WSW-trending structures — Proterozoic weakness zones that provoked the development of sedimentary basins along the southeastern Brazil continental rift. This reactivation is well documented in southern and southeastern Brazil (Riccomini 1989, Salamuni *et al*. 2003, Souza *et al*. 2008, Franco-Magalhães *et al*. 2010a, 2010b).

Thermochronological records (Souza *et al*. 2008) also indicate a subsequent pulse related to the strike-slip reactivation of the NW-SE-, WNW-ESE-, and NNW-SSE-trending fault planes between Oligocene and Miocene (tectonic pulse II; Fig. 17B). In Central Andes, alternation of short extension and long compression periods is observed since the Pliocene (Noblet *et al*. 1996). To this age, we attribute the third deformation pulse with (σ_1) NNW-SSE direction of compression interpreted to have taken place in the TAC (tectonic pulse III; Fig. 17C). The tectonic pulse that started in the Neogene is possibly related to the reorganization of the South American Plate during the Quetchuan event (Frutos 1981, Sebier *et al*. 1988, Cogné *et al*. 2011, 2012), given the development of the compressional deformation (σ_1) that varied from NNW-SSE (Plio-Pleistocene) to NW-SE to WNW-ESE/ENE-WSW trending — Pleistocene-Holocene — (tectonic pulse IV; Fig. 17D) with anticlockwise rotation of (σ_1) paleostress field.

Figure 18 shows the chronological correlation between the post-cretaceous tectonic events of the TAC, so the tectonic pulses defined in this research, determined by relevant field data, can be compared to previously published data, like thermochronological AFT data and syn-magmatic tectonics data (Comin-Chiaramonti *et al*. 2001, Hadler *et al*. 2001, Siga Jr. *et al*. 2007, Franco-Magalhães *et al*. 2010a). The major families of faults, obtained from stereonet statistical analysis, are also shown in Figure 18 as a synthesis of the structural-tectonic evolution of the TAC, in addition to Figure 17.

According to our research, the sequence of tectonic pulses (Figs. 16 and 17) is related to thermotectonic pulses (Cogné *et al*. 2012, Karl *et al*. 2013, Oliveira *et al*. 2016a, 2016b, Oliveira and Jelinek 2017) that resulted in post-breakup tectono-magmatic activities in the Brazilian passive continental margin. The Upper Cretaceous/Paleogene alkaline intrusions, the Paleogenic onshore basins, and the two cooling events dated from the Paleogene and Neogene materialize the tectonic pulses addressed in this research. Such events were partly synchronous with Andean tectonics, providing further evidence that the South American Plate is under a lateral compressive stress that has activated more susceptible older structures (Cogné *et al*. 2012).

The morphostructural and aeromagnetometric lineaments are in good correlation with faults observed in the field. The lineaments oriented to NE-SW trend correspond to reactivation of Proterozoic faults and foliations, with nucleation of secondary structures, whereas lineaments oriented in the N50-70W strike are related to the São Jerônimo-Curiúva Lineament; therefore, the lineament map (Fig. 6) and field data of the TAC show that the NE-SW-trending sinistral faults form conjugated pairs with the NW-SE-trending dextral faults (tectonic pulse III). In contrast, the NW-SE-trending dextral faults were displaced by NNW-SSE (σ_1) stress (tectonic pulse posterior to the formation of structures approximately in E-W trending being possibly present). These two deformation pulses follow a NW-SE to WNW-ESE (σ_1) stress (tectonic pulse IV) that reactivates the N30E-striking dextral faults that, in turn, displaced previous structures.

CONCLUSIONS

The TAC is part of the set of alkaline complexes inserted in the Curitiba-Maringá Fault Zone, oriented in the N45-65W direction and represents a key area for the understanding of the post-Campanian tectonic pulse sequence in the Ponta Grossa Arch domain.

At least 10 families of recurrent faults can be identified in the complex:

- N50E- and N70-80E-striking normal or transtensional faults;
- N30-40E-striking dextral transtensional faults;
- N50-70E-striking sinistral strike-slip and transtensional faults;
- N70-80E-striking sinistral and/or dextral strike-slip faults;
- N20-30W-striking dextral strike-slip, dextral and sinistral transtensional faults;
- N40-60W-striking sinistral strike-slip and dextral and sinistral transtensional faults;

- N60-70E-striking dextral transtensional and sinistral strike-slip faults;
- N80E-striking dextral transtensional faults;
- N70-80W-striking strike-slip and transtensional faults;
- E-W-striking sinistral and/or dextral transtensional faults.

In the field, the most outstanding faults are oriented in the N30-40W and N50-70E and, secondarily, in the N20-30W, N70-90E, and N70-90W directions.

Given the homogeneous rheologic behavior of its lithotypes, the ~83 Ma of the TAC is a favorable site for studying post-Cretaceous tectonics.

Part of its structures exerts control over the relief and drainage. The development of drainage anomalies is specially favored at sites where lineaments intersect, which identifies the development of local morphotectonic processes.

The post-intrusion tectonic data of the TAC allowed the detailing of Cenozoic brittle deformation in the TAC. Such data corroborated similar studies of other alkaline complexes in southern and southeastern Brazil. The tectonic pulses that affected the complex have regional counterparts, likewise in the NW-SE extension associated to the onset and evolution of Paleogene sedimentary basins. As such, our study may contribute to the refinement of previously published Tectonic Models, integrating research results in nearby areas.

The four tectonic pulses result from four different (σ_1) paleostress fields whose relative ages relate to those identified in previous studies on the Cenozoic tectonics of southern and southeastern Brazil.

We proposed a relative chronological order for the tectonic pulses and their respective major stress fields that were based on the geometric relations among faults and secondary structures, which were correlated with thermochronological and tectonic data from previous studies and correlations with data from the Central Andes region:

- Tectonic pulse I: A deformation pulse between the Eocene and Oligocene related to the NW-SE (σ_3) paleostress field with associated vertical to subvertical stress (σ_1) that caused normal reactivation of the N50E- and N70-80E-striking faults. It is also possible that it has reactivated anisotropies formed by pervasive N30-50E-striking basement foliations;
- Tectonic pulse II: Oligo-Miocene deformation pulse related to the NE-SW (σ_1) compression field that caused dextral reactivation of the N30E-striking faults and sinistral strike-slip reactivation of the N70-80W-striking faults, in both cases with a transtensional feature;
- Tectonic pulse III: Plio-Pleistocene deformation pulse related to the N-S to NNW-SSE (σ_1) compression that caused mainly dextral reactivation of the early N40-60W-striking faults and sinistral reactivation of the early NE-SW-striking faults. It also caused nucleation of the N10E-striking sinistral faults;
- Tectonic pulse IV: Pleistocene-Holocene neotectonic deformation pulse related to a (σ_1) compression field between NW-SE and WNW-ESE that caused reactivation of the N70-80W-striking dextral and the N20W-striking sinistral strike-slip faults, with local dextral reactivation of the N30E- and the E-W-striking strike-slip faults. In this deformation pulse, the major compression axis (σ_1) which could explain the presence of striae and steps, both indicative of dextral displacement on faults plane filled with neoformed clay minerals. Some NW-SE-trending fault families show striae with dip angles of up to 50° that reveal an oblique normal component responsible for transtensional faults.

In terms of rheology, the TAC is homogeneous and more competent than the related country rocks, being considered as the border of the crustal weakness zone marked by the Ponta Grossa Arch axis. Such characteristics favored nucleation of faults within the complex and development of trellis patterns in the fluvial network.

The brittle structural framework of the complex resulted from dissipation of paleostress fields that nucleated new families of faults or that nucleated faults correlated to those of the country rocks by reactivating previously existing faults. Reactivation of weakness zones displaced during subsequent deformation pulses according to the orientation of paleostress axes was also considered.

In regionally terms, the initial deformation of the TAC (tectonic pulse I) was probably related to extensional pulses from the Late Cretaceous and Early Paleogene, which caused the development of rift basins in southern and southeastern Brazil. In contrast, compared to other Late Cretaceous complexes, alkaline massifs or domes, such as the Passa Quatro Alkaline Massif, the Lages Dome, and the Cananéia Massif, the TAC shows correlation between compressional pulses that resulted in directional deformation and nucleation of oblique strike-slip faults.

The last deformation pulse (tectonic pulse IV), in turn, aligns with the current deformation of the Brazilian platform, which is given by the (σ_1) NW-SE/E-W stress field directions in the South American Plate. In general terms, our research provides a correlation of Cenozoic tectonics between southern and southeastern Brazil from the study of alkaline massifs and would also explain the occurrence of low-magnitude earthquakes in the region.

The research indicated that considering their recent age and homogeneity of lithotypes, alkaline rocks are important sites for studying and understanding the tectonic evolution of the Brazilian platform during the Cenozoic, particularly in the case of Curitiba-Maringá Fault Zone local paleostress. The proposed tectonic model for the TAC may also have applications in studies aimed at mineral prospecting and groundwater research in the adjacent basement units, as well as in the exploration of hydrocarbons in the arch domain within the continental shelf.

ACKNOWLEDGMENTS

The authors acknowledge the Post-graduate Program in Geology (PPGeol-UFPR) and the Department of Geology (DEGEOL-UFPR) of the Universidade Federal do Paraná for the provision of financial support and infrastructure, the Mineral and Rock Analysis Laboratory of the Universidade Federal do Paraná (LAMIR-UFPR) for the SEM-EDS analysis, the Applied

Geophysical Research Laboratory of the Universidade Federal do Paraná (LPGA-UFPR) for the geoprocessing aeromagnetic data, and to the editors and reviewers of this manuscript for their careful reading and discussions that improved the quality of the text. We are also grateful to the Coordination for the Improvement of Higher Education Personnel (CAPES) for financial support to William Rudolf Lopes Peyerl and Viviane Barbosa Gimenez; and National Council for Scientific and Technological Development (CNPq) for Research Grant PQ-2 to Eduardo Salamuni (process: 307738/2019-1).

ARTICLE INFORMATION

Manuscript ID: 20210053. Received on: 4 JUNE 2021. Approved on: 18 APR 2022.

How to cite this article: Farias T.F.S., Salamuni E., Peyerl W.R.L., Gimenez V.B. Post-Cretaceous brittle tectonics in the Tunas Alkaline Complex, Paraná, Brazil. *Brazilian Journal of Geology*, **52**(3): e20210041, 2022. https://doi.org/10.1590/2317-4889202220210041.

T.F.: formulated the hypothesis; collected field data; wrote the first draft of the manuscript; performed the first structural and laboratory analyses; created the main figures and developed the Discussion chapter. E.S.: helped to formulate the hypothesis; participated in field work helping in data collection; revised the manuscript; analyzed and revised the results of the analyses and wrote part of the Discussion; revised the figures and the manuscript in its final form. W.P.: participated in the fieldwork helping in data collection; revised the manuscript; helped in the formulation of Figures 7, 8, 15 and 16; reviewed the Results chapter. V.G.: revised the text for technical corrections; translated the text into English; revised Figures 17 and 18 as well as the annexes.

Competing interests: the authors declare no competing interests.

REFERENCES

Almeida F.F.M. 1967. Origem e evolução da plataforma brasileira. Rio de Janeiro: DNPM/DGM, **241**:36.

Almeida J., Dios F., Mohriak W.U., Valeriano C.D.M., Heilbron M., Eirado L.G., Tomazzoli E. 2013. Pre-rift tectonic scenario of the Eo-Cretaceous Gondwana break-up along SE Brazil–SW Africa: insights from tholeiitic mafic dyke swarms. *Geological Society*, **369**(1):11-40. https://doi.org/10.1144/SP369.24

Amaral G. 1982. *O arco de Ponta Grossa: uma proposta para a sua configuração e evolução a partir da interpretação de dados de sensoriamento remoto*. MS Dissertation, Inpe, São José dos Campos, 155 p.

Angelier J., Mechler P. 1977. Sur une méthode graphique de recherché dês constraints principales également utilizable en tectonique et en séismologie: la méthode dês dièdres droits. *Bulletin de la Société Géologique de France*, **19**:1309-1318. https://doi.org/10.2113/gssgfbull.S7-XIX.6.1309

Assumpção M., Dias F.L., Zevallos I., Naliboff J.B. 2016. Intraplate stress field in South America from earthquake focal mechanisms. *Journal of South American Earth Sciences*, **71**:278-295. https://doi.org/10.1016/j.jsames.2016.07.005

Assumpção M., Ferreira J., Barros L., Bezerra H., França G.S., Barbosa J.R., Menezes E., Ribotta L.C., Pirchiner M., Nascimento A., Dourado J. 2014. Intraplate seismicity in Brazil: Intraplate Earthquakes. *In*: Talwani P. (Ed.). *Intraplate seismicity*. Cambridge: Cambridge University Press, p. 50-71.

Assumpção M., Schimmel M., Escalante C., Barbosa J.R., Rocha M., Barros L.V. 2004. Intraplate seismicity in SE Brazil: stress concentration in lithospheric thin spots. *Geophysical Journal International*, **159**(1):390-399. https://doi.org/10.1111/j.1365-246X.2004.02357.x

Baêta R.M., Vasconcellos E.M.G. 2004. Caracterização Faciológica das rochas ornamentais do Complexo Alcalino de Tunas/PR. *Boletim Paranaense de Geociências*, **54**:1-22.

Brito-Neves B.B. 1992. O fenômeno da ativação no contexto da tectônica global. *Boletim IG-USP. Série Didática*, (4). 174 p. https://doi.org/10.11606/issn.2316-896X.v0i4p1-174

Castro L.G., Ferreira F.J.F. 2015. Arcabouço geofísico-estrutural da porção meridional do Cinturão Ribeira. *Brazilian Journal of Geology*, **45**(4):449-516. https://doi.org/10.1590/2317-4889201520150007

Centro de Sismologia da USP (Sismo-IAG-USP). 2018. *Últimos eventos significativos*. São Paulo: Centro de Sismologia da USP. Available at: http://www.sismo.iag.usp.br/. Access in: May 2008.

Chavez-Kus L., Salamuni E. 2008. Evidência de tensão N-S intraplaca no Neógeno, Complexo Atuba - região de Curitiba. *Revista Brasileira de Geociências*, **38**(3):439-454. https://doi.org/10.25249/0375-7536.2008383439454

Chiessi C.M., Riccomini C. 2003. Análise morfométrica aplicada à caracterização morfotectônica do Maciço Alcalino de Passa Quatro (SP-MG-RJ). *In*: Simpósio Nacional de Estudos Tectônicos. *Boletim de Resumos*, p. 273-275.

Cobbold P.R., Meisling K.E., Mount V.S. 2001. Reactivation of an obliquely rifted margin, Campos and Santos basins, southeastern Brazil. *AAPG Bulletin*, **85**(11):1925-1944. https://doi.org/10.1306/8626D0B3-173B-11D7-8645000102C1865D

Cogné N., Gallagher K., Cobbold P.R. 2011. Post-rift reactivation of the onshore margin of southeast Brazil: Evidence from apatite (U–Th)/He and fission-track data. *Earth and Planetary Science Letters*, **309**(1-2):118-130. https://doi.org/10.1016/j.epsl.2011.06.025

Cogné N., Gallagher K., Cobbold C., Riccomini C., Gautheron C. 2012. Postbreakup tectonicsin southeast Brazil from thermochronological data and combined inverse-forward thermal history modeling. *Journal of Geophysical Research, American Geophysical Union*, **117**(B11). https://doi.org/10.1029/2012JB009340

Comin-Chiaramonti P., Gomes C.B., Ruberti E., Antonini P., Castorina F., Censi P. 2001. Mato Preto Alkaline-Carbonatite Complex: Geochemistry and isotope (O-C, Sr-Nd) constrains. *Geochimica Brasiliensis*, **15**(1-2):23-34.

Coutinho J. 2008. Enxame de diques da junção tríplice do Paraná, Brasil meridional. *Geologia USP. Série Científica*, **8**(2):28-52. https://doi.org/10.5327/Z1519-874X2008000200003

Crosby T.B., Whipple K.X. 2006. Knickpoint initiation and distribution within fluvial networks: 236 waterfalls in the Waipaoa River, North Island, New Zealand. *Geomorphology*, **82**(1-2):16-38. https://doi.org/10.1016/j.geomorph.2005.08.023

Delvaux D. 2012. Release of program Win-Tensor 4.0 for tectonic stress inversion: statistical expression of stress parameters. *Geophysical Research Abstracts*, **14**, 2 p. Available at: https://www.researchgate.net/publication/258618974_Release_of_program_WinTensor_40_for_tectonic_stress_inversion_statistical_expression_of_stress_parameters. Accessed in: June, 2018.

Di Giorgio D. 2003. *Fatores geológicos no planejamento de lavra de rocha ornamentais*. MS Dissertation. Universidade Federal do Rio Grande do Sul, Porto Alegre, 148 p.

Doblas M. 1998. Slickenside kinematic indicators. *Tectonophysics*, **295**(1-2):187-197. https://doi.org/10.1016/S0040-1951(98)00120-6

Engelmann de Oliveira C.H., Jelinek A.R., Timoteo D., Bernet M. 2018. Thermotectonic history of the Maastrichtian reservoir in Campos Basin.

Marine and Petroleum Geology, **93**:331-343. https://doi.org/10.1016/j.marpetgeo.2018.03.021

Fassbinder E., Sadowski G.R., Fiori A.P. 1992. Análise estrutural da falha da Lancinha no estado do Paraná. *In*: Congresso Brasileiro de Geologia, 37., 1992, São Paulo. *Congress Proceedings*, **2**:362-363.

Ferreira F.J.F. 1982. Lineamentos estruturais-magnéticos da região centro-oriental da Bacia do Paraná e seu significado tectônico. *In*: Geologia da Bacia do Paraná. Reavaliação da potencialidade e prospectividade em hidrocarbonetos. *Paulipetro, Consórcio CESP-IPT*, 144-166.

Ferreira F.J.F., Moraes R.A.V., Ferrari M.P., Vianna R.B. 1981. Contribuição ao estudo do Lineamento Estrutural de Guapiara. *In*: Simpósio Regional de Geologia, 3., 1981, Curitiba. *Minutes*, **1**:226-240.

Ferreira F.J.F., Souza J., Bongiolo A.B.S., Castro L.G. 2013. Enhancement of the total horizontal gradient of magnetic anomalies using the tilt angle. *Geophysics*, **78**(3):J33-J41. https://doi.org/10.1190/geo2011-0441.1

Ferreira F.J.F., Souza J., Bongiolo A.B.S., Castro L.G., Romeiro M.A.T. 2010. Realce do gradiente horizontal total de anomalias magnéticas usando a inclinação do sinal analítico. Parte I: Aplicação a dados sintéticos. *In*: Simpósio Brasileiro de Geofísica, 4., 2010. *Abstract Bulletin*, **1**:1-6.

Fiori A.P. 1994. Evolução geológica da Bacia Açungui. *Boletim Paranaense de Geociências*, **42**:7-27.

Fiori A.P. Fassbinder E., Rabelo L. 1998. Geologia da Região de Tunas -Paraná, Brasil. *Boletim Paranaense de Geociências*, **46**:141-150.

Franco-Magalhães A.O.B., Hackspacher P.C., Glasmacher U.A., Saad A.R. 2010a. Rift to post-rift evolution of a "passive" continental margin: the Ponta Grossa Arch, SE Brazil. *International Journal of Earth Science*, **99**(7):1599-1613. https://doi.org/10.1007/s00531-010-0556-8

Franco-Magalhães A.O.B., Hackspacher P.C., Saad A.R. 2010b. Exumação tectônica e reativação de paleolineamentos no Arco de Ponta Grossa: termocronologia por traços de fissão em apatitas. *Revista Brasileira de Geociências*, **40**(2):184-195.

Frutos J. 1981. Andean tectonics as consequence of sea-floor spreading. *Tectonophysics*, **72**(1-2):T21-T32. https://doi.org/10.1016/0040-1951(81)90082-2

Fuck A.F. 1972. *Geologia do Maciço Alcalino de Tunas, Paraná, Brasil*. PhD Thesis. Universidade de São Paulo, São Paulo, 82 p.

Gallagher K., Hawkesworth C.J., Mantovani M.S.M. 1994. The denudation history of the onshore continental margin of SE Brazil inferred from Apatite Fission Track data. *Journal of Geophysical Research*, **99**(B9):18117-18145. https://doi.org/10.1029/94JB00661

Gomes C.B., Azzone R.G., Ruberti E., Vasconcelos P.M., Kei S., Rojas G.E.E. 2018. New age determinations for the Banhadão and Itapirapuã Complexes in the Ribeira Valley, southern Brazil. *Brazilian Journal of Geology*, **48**(2):403-414. https://doi.org/10.1590/2317-4889201820170094

Gomes C.B., Barbieri M., Beccaluca L., Brotzu P., Conte A., Rubert E., Sheibe F., Tamura R.M., Traversa G. 1987. Petrological and geochemical studies of alkaline rocks from continental Brazil. 2. The Tunas massif, State of Paraná. *Geochimica Brasiliensis*, **1**(2):201-234.

Gomes C.B., Ruberti E., Comin-Chiaramonti P., Azzone R.G. 2011. Alkaline magmatism in the Ponta Grossa Arch, SE Brazil: a review. *Journal of South American Earth Sciences*, **32**:152-168.

Hackspacher P.C., Ribeiro L.F.B., Ribeiro M.C.S., Fetter A.H., Neto J.C.H., Tello C.E.S., Dantas E.L. 2004. Consolidation and Break-up of the South American Platform in Southeastern Brazil: Tectonothermal and Denudation Histories. *Gondwana Research*, **7**(1):91-101. https://doi.org/10.1016/S1342-937X(05)70308-7

Hadler J.C., Tello C.A., Lunes P.J., Guedes S., Paulo S.R., Hackspacher P., Ribeiro L.F.B. 2001. Método de traços de fissão em apatita-1: uma metodologia para avaliar histórias térmicas e hidrocarbonetos. *In*: Congresso Brasileiro de P&D em Petróleo e Gás, 1. 2001. *Abstract Bulletin*. UFRN: Natal.

Hasui Y. 1990. Neotectônica e aspectos fundamentais da tectônica ressurgente no Brasil. *In*: Workshop sobre Neotectônica e Sedimentação Cenozoica Continental no Sudeste Brasileiro, 1., 1990. *Bulletin*, **11**:1-31.

Hiruma S.T., Riccomini C., Modenesi-Gauttieri M.C. 2001. Neotectônica do Planalto de Campos do Jordão, SP. *Revista Brasileira de Geociências*, **31**(3):347-356.

Hiruma S.T., Riccomini C., Modenesi-Gauttieri M.C., Hackspacher P.C., Hadler Neto H.N., Franco-Magalhães A.O.B. 2010. Denudation history of the Bocaina Plateau, Serra do Mar, southeastern Brazil: Relationships to Gondwana breakup and passive margin development. *Gondwana Research*, **18**(4):674-687.

Jacques P., Machado R., Nummer A. 2010. Lineamentos estruturais na borda leste da Bacia do Paraná em Santa Catarina: análise multiescala com base em imagens LANDSAT e SRTM. *Pesquisas em Geociências*, **37**(2):117-131. https://doi.org/10.22456/1807-9806.22653

Karl M., Glasmacher U.A., Kollenz S., Franco-Magalhaes A.O.B., Stockli D.F., Hackspacher P.C. 2013. Evolution of the South Atlantic passive continental margin in southern Brazil derived from zircon and apatite (U–Th–Sm)/He and fission-track data. *Tectonophysics*, **604**:224-244. https://doi.org/10.1016/j.tecto.2013.06.017

Lima C.C.U. 2000. O Neotectonismo na Costa do Sudeste e do Nordeste Brasileiro. *Revista de Ciência & Tecnologia*, **15**:91-102.

Machado R., Roldan L.F., Jacques P.D., Fassbinder E., Nummer A.R. 2012. Tectônica transcorrente Mesozoica-Cenozoica no Domo de Lages – Santa Catarina. *Revista Brasileira de Geociências*, **42**(4):799-811. https://doi.org/10.5327/Z0375-75362012000400011

Mancini F., Riccomini C. 1994. Estilos estruturais da Formação Pindamonhangaba, Bacia de Taubaté, SP. *In*: Congresso Brasileiro de Geologia, Balneário de Camboriú. *Expanded Summaries Bulletin*, **1**:564-565.

Modica J.C., Brush E. 2004. Postrift sequence stratigraphy, paleogeography, and fill history of the deep-water Santos Basin, offshore southeast Brazil. *AAPG Bulletin*, **88**(7):923-945. https://doi.org/10.1306/01220403043

Morales N., Hasui Y., Souza I.A., Antonialli R.C. 2017. Reconstrução de eixos de paleotensão a partir de populações de falhas na região sudeste do Brasil. *In*: Congresso Brasileiro de Geologia, 48., 2017. *Congress proceedings*. Available at: http://cbg2017anais.siteoficial.ws/st15/ID6867_111952_52_paleotensoes.pdf. Accessed in: Feb, 2019.

Moura T.T., Riccomini C. 2017. Estruturas transversais às bacias de Taubaté e Resende: natureza e possível continuidade na bacia de Santos, Brasil. *In*: Congresso Brasileiro de Geologia, 48., 2017. *Congress proceedings*. Available ay: http://cbg2017anais.siteoficial.ws/st26/ID5107_110187_52_110187_52_Resumo_Thai_s_TM_CBG.pdf. Accessed in: July, 2018.

Noblet C., Lavenu A., Marocco R. 1996. Concept of continuum as opposed to periodic tectonism in the Andes. *Tectonophysics*, **255**(1-2):65-78. https://doi.org/10.1016/0040-1951(95)00081-X

Nummer A.R., Machado R., Jacques P.D. 2014. Tectônica transcorrente mesozoica/cenozoica na porção leste do Planalto do Rio Grande do Sul, Brasil. *Pesquisas em Geociências*, **41**(2):121-130. https://doi.org/10.22456/1807-9806.78078

Obsis. 2018. Últimos eventos naturais. Available at: http://obsis.unb.br/portalsis/. Accessed in: Jan, 2018.

O'Leary D.W., Freidman J.D., Pohn HA. 1976. Lineament, linear, lineation: Some proposed new definitions for old terms. *Geological Society of America Bulletin*, **87**(10):1463-1469. https://doi.org/10.1130/0016-7606(1976)87%3C1463:LLLSPN%3E2.0.CO;2

Oliveira C.H.E., Jelinek A.R. 2017. História termotectônica da margem continental brasileira a partir de dados de traços de fissão em apatita. *Pesquisas em Geociências*, **44**(3):387-400. https://doi.org/10.22456/1807-9806.83263

Oliveira C.H.E., Jelinek A.R., Chemale Jr. F., Bernet, M. 2016a. Evidence of post-Gondwana breakup in Southern Southern Brazilian Shield: Insights from apatite Ana zircon fission track thermochronology. *Tectonophysics*, **666**:173-187.

Oliveira C.H.E., Jelinek A.R., Chemale Jr. F., Cupertino J.A. 2016b. Thermotectonic history of the southeastern Brazilian margin: Evidence from apatite fission track data of the offshore Santos Brasilian continental basement. *Tectonophysics*, **685**:21-34. https://doi.org/10.1016/j.tecto.2016.07.012

Petit J.P. 1987. Criteria for the sense of movement on fault surfaces in brittle rocks. *Journal of Structural Geology*, **9**(5-6):597-608. https://doi.org/10.1016/0191-8141(87)90145-3

Peyerl W.R.L., Salamuni E., Sanches E., Nascimento E., Santos J., Gimenez V., Silva C., Farias T. 2018. Reativation of Taxaquara Fault and its morphotectonic influence on the Jordão River catchment, Paraná. *Brazilian Journal of Geology*, **48**(3):553-573. https://doi.org/10.1590/2317-4889201820170110

Riccomini C. 1989. *O rift continental do sudeste do Brasil*. PhD Thesis. Instituto de Geociências, Universidade de São Paulo, São Paulo, 256 p.

Riccomini C. 1995. Padrão de fraturamentos do maciço alcalino de Cananéia, estado de São Paulo: relações com a tectônica mesozóico-cenozóica do Sudeste do Brasil. *Revista Brasileira de Geociências*, **25**(2):79-84.

Riccomini C., Assumpção M. 1999. Quaternary Tectonics in Brazil. *Episodes*, **22**(3):221-225. https://doi.org/10.18814/epiiugs/1999/v22i3/010

Riccomini C., Pellogia A.U.G., Saloni J.C.L., Kohnke M.W., Figueira R.M. 1989. Neotectonic activity in the Serra do Mar rift system (Southeastern Brazil). *Journal of South American Earth Science*, **2**(2):191-197. https://doi.org/10.1016/0895-9811(89)90046-1

Riccomini C., Sant'Anna L.G., Ferrari A.L. 2004. *Evolução geológica do rift continental do sudeste do Brasil. In*: Mantesso-Neto V. (Ed.). *Geologia do continente sul-americano:* evolução e obra de Fernando Flávio Marques de Almeida, p. 383-405.

Rugenski A. 2006. *Investigação geofísica dos complexos alcalinos do Sul e Sudeste do Brasil*. PhD Thesis, Universidade de São Paulo, São Paulo.

Sadowski G.R., Motidome M.J. 1987. Brazilian Mega Faults. *Revista de Geologia*, **31**:61-75.

Salamuni E., Ebert H.D., Borges M.S., Hasui Y., Costa J.B.S., Salamuni R. 2003. Tectonics and sedimentation of the Curitiba Basin. *Journal of South American Earth Sciences*, **15**(8):901-910. https://doi.org/10.1016/S0895-9811(03)00013-0

Salamuni E., Ebert H.D., Hasui Y. 2004. Morfotectônica da Bacia Sedimentar de Curitiba. *Revista Brasileira de Geociências*, **34**(4):469-478.

Salamuni E., Salamuni R., Ebert H.D. 1999. Contribuição à geologia da Bacia Sedimentar de Curitiba. *Boletim Paranaense de Geociências*, **47**:123-142.

Salazar-Mora C.A., Campanha G.A.C., Wemme, K. 2013. Microstructures and K-Ar illite fine fraction ages of the cataclastic rocks associated to the Camburu Shear Zone, Ribeira Belt, Southeastern Brazil. *Brazilian Journal of Geology*, **43**(4):607-622. https://doi.org/10.5327/Z2317-48892013000400003

Salvador E., Riccomini R. 1995. Neotectônica da região do alto estrutural de Queluz (SP-RJ, Brasil). *Revista Brasileira de Geociências*, **25**(3):151-164.

Santos J.M., Salamuni E., Silva C.L., Sanches E., Gimenez V., Nascimento E.R. 2019. Morphotectonics in the Central-East Region of South Brazil: Implications for Catchments of the Lava-Tudo and Pelotas Rivers, State of Santa Catarina. *Geomorphology*, **328**:138-156. https://doi.org/10.1016/j.geomorph.2018.12.016

Sebier M., Lavenu A., Fornari M., Soulas J.P. 1988. Tectonics and uplift in Central Andes (Peru, Bolivia, and Northern Chile) from Eocene to present. *Géodynamique*, **3**(1-2):85-105.

Serviço Geológico do Brasil (CPRM). 2011. Relatório final do levantamento e processamento dos dados magnetométricos e gamaespectrométricos. *Programa Geologia do Brasil (PGB):* Projeto aerogeofísico Paraná – Santa Catarina, (**I**). 88 p.

Siga Jr. O., Gomes C.B., Sato K., Passarelli C.R. 2007. O Maciço Alcalino de Tunas, PR: novos dados geocronológicos. *Geologia USP. Série Científica*, **7**(2):71-80. https://doi.org/10.5327/Z1519-874x2007000200005

Silva T.P., Mello C.L. 2011. Reativações Neotectônicas na Zona de Cisalhamento do Rio Paraíba do Sul (Sudeste do Brasil). *Geologia USP. Série Científica*, **11**(1):95-111. https://doi.org/10.5327/Z1519-874X2011000100006

Siqueira-Ribeiro M.C., Hackspacher P.C., Ribeiro L.F.B., Hadler Neto J.C. 2012. Evolução Tectônica e Denudacional da Serra do Mar (SE/BRASIL) no limite entre o Cretaceo Superior e Paleoceno utilizando análises de Traços de Fissão e U-TH/HE em Apatitas. R*evista Brasileira de Geomorfologia*, **12**:3-14. https://doi.org/10.20502/rbg.v12i0.254

Souza I.A. 2008. *Falhas de transferência da porção norte da Bacia de Santos interpretada a partir de dados sísmicos: sua influência na evolução e deformação da bacia*. MS Dissertation. Universidade Estadual Paulista Júlio Mesquita Filho, Rio Claro, 156 p.

Souza I.A., Ebert H.D., Castro J.C., Soares Jr. A.V., Silva G.H.T.S., Benvenutti C.F. 2008. Caracterização das falhas de transferência na porção norte da Bacia de Santos a partir da integração de dados geológicos e geofísicos. *Boletim de Geociências da Petrobras*, **17**(1):109-132.

Souza P.C.M. 2011. *Análise cinemática e dinâmica dos sistemas de falhas Cenozoicas ENE-WSW do entorno da Laguna de Araruama (RJ)*. MS Dissertation. Universidade Federal do Rio de Janeiro, Rio de Janeiro. Available at: https://www.geologia.ufrj.br/images/documentos/Teses_e_Disserta%C3%A7%C3%B5es/2011/Disserta%C3%A7%C3%B5es/Pricilla_de_Souza_Mestrado.pdf. Accessed in: May, 2017.

Strugale M., Rostirolla S.P., Mancini F., Portela Filho C.V., Ferreira F.J.F., Freitas R.C. 2007. Structural framework and Mesozoic-Cenozoic evolution of Ponta Grossa Arch, Paraná Basin, southern Brazil. *Journal of South American Earth Sciences*, **24**(2-4):203-227. https://doi.org/10.1016/j.jsames.2007.05.003

Tjia H.D. 1964. Slickensides and fault movements. *Geological Society of America Bulletin*, **75**(7):683-686. https://doi.org/10.1130/0016-7606(1964)75[683:SAFM]2.0.CO;2

Trein E., Marini O.J., Fuck R.A. 1967. Rochas Alcalinas no Primeiro Planalto do Estado do Paraná. *In*: Bigarella J.J., Salamuni R., Pinto V.M. (Eds.). Geologia do Pré-Devoniano e intrusivas subsequentes da Porção Oriental do Estado do Paraná. *Boletim Paranaense de Geociências*, **23-25**:325-347.

Trzaskos B. 2006. *Anisotropia Estrutural de arenitos do Grupo Itararé, Permocarbonífero da Bacia do Paraná*. PhD Thesis. Universidade Federal do Paraná, Curitiba, 160 p.

Vasconcellos E.M.G, Gomes C.B. 1992. Caracterização petrográfica de brechas vulcânicas no Complexo Alcalino de Tunas, PR. *Revista Brasileira de Geociências*, **22**(3):269-274.

Vasconcellos E.M.G, Gomes C.B. 1998. Diques e plugs alcalinos da região do Vale do Ribeira, divisa dos Estados do Paraná e São Paulo: química mineral. *Boletim IG-USP. Série Científica*, **29**:98-124. https://doi.org/10.11606/issn.2316-8986.v29i0p97-124

Velázquez V.F., Riccomini C., Gomes C.B., Kirk J. 2011. The Cretaceous Alkaline Dyke Swarm in the Central Segment of the Asunción Rift, Eastern Paraguay: Its Regional Distribution, Mechanism of Emplacement and Tectonic Significance. *Journal of Geological Research*, **2011**:946701. https://doi.org/10.1155/2011/946701

Zalán P.V., Wolff S., Conceição J.C.J., Astolfi M.A.M., Vieira I.S. 1987. Tectônica e sedimentação da Bacia do Paraná. *In*: Simpósio Sulbrasileiro de Geologia, 3., 1987. *Atas...*, **1**:441-477. Curitiba: SBG.

Will T.M., Frimmel H.E. 2018. Where Dodô a continent prefer to break up? Some lessons from the South Atlantic margins. *Gondwana Research*, **53**:9-19.